A Chaperonin Complex Regulates Organelle Proteostasis in Malaria Parasites

Amanda Tissawak[1,2], Yarden Rosin[1,2], Michal Shahar[1,2], Nirit Trabelsi[1], Ora Furman-Schueler[1], Steven M Johnson[3], Anat Florentin[1,2*].

[1] Department of Microbiology and Molecular Genetics, Faculty of Medicine, The Hebrew University of Jerusalem, Jerusalem, Israel

[2] The Kuvin Center for the Study of Infectious and Tropical Diseases, Faculty of Medicine, The Hebrew University of Jerusalem, Jerusalem, Israel

[3] Department of Biochemistry and Molecular Biology, Indiana University School of Medicine, Indianapolis, IN, USA

[*] **Corresponding Author:** Anat Florentin, +972-2-6757976 (phone), Email: anat.florentin@mail.huji.ac.il

Author Contributions:

Conceived and designed the experiments: AF, AT

Performed the experiments: AF, AT, YR, MS

AF3 computational analysis: NT, OFS

CPN60-1587 structural model generation: SMJ

Analyzed the data: AF, AT, SMJ

Wrote the paper: AF, AT, SMJ

Competing Interest Statement: S.M.J. is a founder of BioEL Inc, which was formed to commercialize GroEL inhibitors for antibacterial applications. The remaining authors declare no competing interests.

Preprint Server: BioRxiv

Classification: Biological Sciences (major), Microbiology (Minor).

Keywords: malaria, *Plasmodium falciparum*, parasitology, apicoplast, proteostasis, chaperonin, CPN, HSP60, Clp system.

This PDF file includes:

Main Text
Figures 1 to 8 (Sup Fig. 1 to 2)
Tables 1 and 2

Abstract

The apicoplast of *Plasmodium* parasites serves as a metabolic hub that synthesize essential biomolecules. Like other endosymbiotic organelles, 90% of the apicoplast proteome is encoded by the cell nucleus and transported to the organelle. Evidence suggests that the apicoplast has minimal control over the synthesis of its proteome and therefore it is unclear how organelle proteostasis is regulated. Here, we identified and investigated a large and conserved chaperonin (CPN) complex with a previously unknown function. Using genetic tools, we demonstrated that its main subunit, CPN60, localizes to the apicoplast and is essential for parasite's asexual replication due to its organellar functions. Unlike its close orthologues in other prokaryotic and eukaryotic cells, CPN60 is not upregulated during heat shock (HS) and does not affect HS response in the parasite. Instead, we found that it is directly involved in proteostasis through interaction with a proteolytic complex called Clp (*caseinolytic protease*) that degrades organellar proteins in a regulated manner. We showed that CPN60 physically binds both the active and inactive forms of the Clp complex, and manipulates its stability. Using computational prediction tools, we modeled the interaction between these two large complexes to understand how a stable interface is attained. Finally, we screened a library of inhibitors for the bacterial CPN60 orthologue GroEL, in order to test the potential of chaperonin inhibition as antimalarial. These inhibitors demonstrated an anti-*Plasmodial* activity that was not restricted to apicoplast function. Taken together, this work reveals how balanced activities of proteolysis and refolding safeguard the apicoplast proteome.

Significance Statement

The cell of the human malaria parasite, *Plasmodium falciparum*, has a unique organelle called the apicoplast that produces essential metabolites. Most apicoplast proteins are encoded by the nucleus and it is unclear how the organelle maintains a stable proteome. Here, we address the question of organelle proteostasis by investigating the function of a large chaperonin complex. We show that it is essential for parasite's viability due to its role in apicoplast functions. We demonstrate that it binds and stabilizes another large proteolytic complex, and further explore its potential as a drug target. This study reveals how balanced refolding and proteolysis safeguard the apicoplast proteome and opens a new avenue for antimalarial drug discovery.

Main Text

Introduction

The malaria parasite, *Plasmodium falciparum*, remains one of the deadliest human pathogens, causing 600,000 deaths yearly worldwide[1]. Limited vaccines efficacies and spreading of drug resistance are major global concerns. Despite years of research, many aspects of the parasite's basic cell biology remain obscure, hindering rational drug design and improved therapeutic interventions. Like most other related parasites from the family of *Apicomplexa*, this single-celled eukaryotic organism contains a non-photosynthetic plastid called apicoplast[2,3]. This unique organelle evolved via a two-step endosymbiosis; in the primary endosymbiotic event, a cyanobacterium was incorporated into a eukaryotic cell to form the modern chloroplast. During the secondary endosymbiotic event, a photosynthetic red alga was further taken up by a protist and led to the formation of a secondary plastid[4]. Although not photosynthetic, the apicoplast harbors essential prokaryotic metabolic pathways that are essential to the parasite throughout its complex life cycle, including fatty acid, Fe-S clusters, and isoprenoids biosynthesis[5]. The *Plasmodium* apicoplast shares molecular features with prokaryotes, plants and parasites, and therefore encompasses multiple parasite-specific drug targets. Indeed, drugs that target apicoplast biology are in clinical use[6]. Most of those drugs (e.g., doxycycline, clindamycin) target the prokaryotic protein synthesis machinery in the apicoplast[6,7]. However, less than 10% of the apicoplast proteome is encoded by its own genome. The vast majority of the hundreds of apicoplast proteins are encoded in the nuclear genome and are transported to the organelle via the secretory pathway[8,9]. Available transcriptomic data suggest that the apicoplast does not control the expression of these nuclear-encoded proteins[10]. In fact, parasites without an apicoplast continue to express and accumulate apicoplast proteins in vesicle-like structures in the cytoplasm[11–14]. Due to the inability of the apicoplast to control its own protein synthesis, it is unclear how the apicoplast maintains a stable proteome. Previously, we suggested that protein degradation may play a central role in organelle proteostasis and showed that apicoplast-targeted Clp (*caseinolytic protease*) proteins form an essential proteolytic complex in the organelle[14,15].

The conserved Clp family consists of proteases and chaperones that form multi-subunit proteolytic complexes, with complex composition varying widely between

different species and organelles[16,17]. In bacteria and plant chloroplasts, the ClpP proteases typically associate with Clp ATPase chaperones that unfold and feed substrates into the ClpP barrel-like cavity for degradation[18–20]. However, the putative *Plasmodium* Clp proteins differ significantly from their bacterial orthologs and their organellar, molecular and enzymatic functions are unclear[21,22]. We have previously shown that the *Plasmodium* ClpC chaperone (PfClpC) is essential for parasite viability and apicoplast biogenesis[14]. We also demonstrated that the highly-active proteolytic Clp subunit, PfClpP, is assembled and activated through trans-autocatalytic activity and is stabilized by the PfClpC chaperone[15]. Despite detailed genetic and molecular data illuminating complex composition, no regulator of the apicoplast Clp complex has been identified.

Besides the Clp chaperones, the *Plasmodium* apicoplast is predicted to host other molecular chaperones, among those, chaperonin 60. This 60 kDa Heat Shock protein, often termed HSP60 or CPN60, is highly conserved and found in nearly all organisms[23]. Its bacterial orthologue, GroEL, is involved in maintaining proteostasis under different stressors[24], and in most eukaryotic cells, *Plasmodium* included, a mitochondrial orthologue is required for organellar protein import[25]. In apicomplexan parasites, a CPN60 homolog was reported to localize to the apicoplast[15,26], although its functions are unknown.

Here, we report the molecular investigation of a non-mitochondrial CPN60 orthologue in the malaria parasite *P. falciparum*. We show that it localizes to the apicoplast and is primarily expressed during the late stages of the parasite's life cycle, when organelle biogenesis occurs. We found that CPN60 function is essential for parasites viability, but unlike its orthologs in most organisms, it is not involved in heat shock response. Instead, it is required for apicoplast functions and colocalizes and interacts with the proteolytic Clp complex. We further demonstrate that it binds the inactive PfClpP zymogen, as well as the mature protease and this interaction is required for Clp complex stability and activity. Lastly, we screened a panel of inhibitors of the bacterial HSP60 orthologue GroEL in order to test the potential of chaperonin inhibition as antimalarial. Taken together, our studies shed light on the activity of the apicoplast CPN60 and its central role in maintaining organelle proteostasis and parasite's viability.

Results

Plasmodium falciparum chaperonin 60 orthologue is essential for parasite's survival due to its function in the apicoplast

Our previous work suggested that the apicoplast employs caseinolytic protease (Clp)-mediated degradation to regulate protein levels and maintain organellar functions[14,15]. In order to further investigate proteostasis regulation in the apicoplast, we performed an affinity screen, immunoprecipitating several different Clp subunits coupled with mass spectrometry analysis[15]. These affinity screens identified several apicoplast proteins potentially interacting with the Clp complex, though their precise biological roles remain unclear. Notably, we found a conserved apicoplast-resident heat shock protein (HSP60) homolog, termed chaperonin 60 (CPN60). To test whether and how CPN60 is involved in proteostasis and other apicoplast functions, we employed a genetic approach using the tetR-Dozi system, a *Plasmodium*-specific method[27] that allows conditional knockdown of CPN60 (Fig. 1A). We tagged the gene with a V5 tag followed by the tetR-Dozi cassette. Using CRISPR/Cas9, we incorporated the regulatory cassette at the 3′ end of the CPN60 gene, creating the CPN60$^{V5\text{-}apt}$ parasite line. Genotyping of independently isolated clones was performed by PCR analysis, and showed correct integration into the *cpn60* locus (Fig. 1B). Western blot analysis revealed expression of endogenous V5-tagged CPN60 at the predicted 85 kDa size. The presence of a double band suggested that CPN60, similar to other apicoplast proteins, contains a transit peptide in its cytoplasmic form (higher band) that is cleaved in the apicoplast-residing protein (lower band) (Fig. 1C). Homologs of the HSP60 family are often considered house keeping proteins, retaining constant expression levels throughout the cell cycle[23]. However, protein extraction from synchronized parasites revealed that CPN60 levels were relatively low at the first 24 hours of the sexual cycle (Fig. 1C). Increased CPN60 protein expression was detected only at the later trophozoite stage, 36 hours post-invasion (hpi), around the time that schizogony (nuclear replication), and apicoplast development begin[28] (Fig. 1C). Unlike CPN60 mRNA levels, which peak at the middle of the parasite's cell cycle (24hpi), quantification of CPN60 protein levels peak towards the end of the cycle at 44 hpi (Fig. 1D and 1E, respectively). While several hours gap between mRNA and protein expression is expected, this

half a cycle discrepancy suggests that transcription is not the sole mechanism controlling apicoplast CPN60 levels.

To look into CPN60 cellular function, we activated the tet-aptamer system, to induce translational repression of CPN60 (Fig. 2A). We induced protein knockdown by removal of the stabilizing ligand anhydrotetracycline (aTC), effectively reducing CPN60 protein levels within 24 hours, dropping below detection after 72 hours (Fig. 2B). The consequences of CPN60 knockdown were parasite's death, indicating that its activity is essential for parasite's viability (Fig. 2C). It was shown that apicoplast-related cytotoxicity can be reversed by addition of isopentenyl pyrophosphate (IPP), an essential apicoplast-producing metabolite[11]. We observed that media supplementation with IPP completely restored mutants' growth, indicating that CPN60 essential activity is restricted to apicoplast function (Fig. 2D). An apicoplast-associated damage typically results in a delayed cell death, as observed in parasites treated with doxycycline or chloramphenicol. Such parasites complete their first 48 hours cell cycle, reinvade new cells and die only at the end of the 2nd cycle after 96 hours of treatment[29]. We therefore synchronized the cultures and removed aTC from early rings stage CPN60$^{V5\text{-}apt}$ parasites and observed their intraerythrocytic development (Fig. 2E). During the first cycle, knockdown parasites developed like +aTC control until the trophozoite stage, but then could not process into normal schizogony (Fig. 2F). The few persisting parasites in the culture could not egress or reinvade and failed to form new ring-stage parasites in the 2nd cycle (Fig. 2G). This indicates that CPN60 ablation results in an apicoplast-immediate cell death.

Plasmodium CPN60 is not involved in heat shock response

In most organisms, HSP60 family members are involved in stress pathways, particularly heat shock (HS) response. During infection, the malaria parasite faces periodic fevers, making HS one of its main stressors. To look into a function of apicoplast CPN60 during HS, we measured its expression levels following 24 hours incubation at 40°c. *Wildtype* parasites subjected to HS, grew slower and exhibited morphological defects (Fig. 3A). Western blot analysis (Fig. 3B) and quantification (Fig. 3C) did not detect a significant increase in CPN60 protein levels. Next, we sought to analyze the effect of CPN60 depletion on parasite's survival following HS. Because complete knockdown of CPN60 leads to parasite's death, we were interested in decreasing CPN60 levels to the point where subtle effects could be

tested. To do that, we performed a half-maximal effective concentration (EC50) assay for aTC, and found that 4.3 nM support 50% survival (Fig. 3D). We performed the same EC50 assay following incubation at 40ºc, and observed a similar EC50 dose of 5 nM (Fig. 3E). Next, we measured CPN60 protein levels while growing the parasite's with 2X EC50 dose (8 nM aTC) compared to the its levels in non-induced parasites which are cultured at 100X EC50 (500 nM aTC, Fig. 3F). Quantification of this western blot revealed that at this aTC concentration, CPN60 cellular levels were decrease by 50% (Fig. 3G). Next, we measured parasite's growth following 24 hours incubation at 40ºc. While *wildtype* parasites recover after this heat exposure, their growth is slightly attenuated (Fig. 3H, blue curve). Importantly, parasites with reduced CPN60 levels (Fig. 3H, 16, 8, 4 nM are purple, green and red curves, respectively) exhibited compromised growth, in an aTC dose-dependent manner. However, exposure to heat did not alter their relative growth compared to the effect it had on *wildtype* parasites (Fig. 3H). Collectively, these data suggest that unlike canonical CPN60 orthologues, the *Plasmodium* CPN60 is not involved in heat shock response and rather possesses an apicoplast-specific function.

Co-expression and co-localization of CPN60 and PfClpP, the active protease of the Clp complex

Previously, we identified CPN60 in a mass spectrometry screen as a potential interactor of the Clp complex[15]. To look deeper into this potential interaction, we expressed a tagged copy of the Clp protease subunit, PfClpP. PfClpP is a highly potent protease and in order to avoid toxic effects, we used a transgenic PfClpP with a point mutation in its proteolytic active site (S264A), rendering it catalytically inactive[15]. Furthermore, we designed integration into the parasite's genome under the endogenous *hsp110* promoter, which enables constant but moderate levels of expression[15]. This construct was transfected on the background of the CPN60 conditional mutants, generating the CPN60$^{V5\text{-}apt}$; ClpP$^{DEAD\text{-}Ty}$ parasite line (Fig. 4A). Clones were isolated and integration at the *hsp110* locus was verified using diagnostic PCR (Fig. 4B). Western blot demonstrated the co-expression of the endogenous CPN60^{V5} at 85 KDa, as well as the transgenic ClpP$^{DEAD\text{-}Ty}$ (Fig. 4C). The expected processing pattern of PfClpP is consistent with a model of a full-length PfClpP, presumably in transit through the secretory pathway (fraction III), an apicoplast-localized PfClpP (fraction II), and a mature PfClpP after proteolytic

removal of an inhibitory pro-domain (fraction I) (Fig. 4D). Immunofluorescent microscopy, revealed that CPN60 co-localizes with PfClpP in the apicoplast (Fig. 4E). We verified that expression of ClpP$^{DEAD\text{-}Ty}$ had no effect on parasite's growth or CPN60 function, as can be seen by a consistent EC50 of 4.5 nM aTC (Fig. 4F). We also verified that ClpP$^{DEAD\text{-}Ty}$ expression had no effect on parasite's growth or CPN60 function following HS (Fig. 4G). We concluded that ectopic expression of ClpP$^{DEAD\text{-}Ty}$ does not affect its processing or overall apicoplast morphology. Furthermore, it colocalizes with CPN60 without affecting its activity, indicating that the co-expression could be used to evaluate interaction between the two.

Physical interaction between the apicoplast Chaperonin and Clp complexes

To test for physical interactions between CPN60 and PfClpP, we performed immunoprecipitation using the double-mutant parasites. The pulldown of ClpP$^{DEAD\text{-}Ty}$ resulted in the Co-IP of CPN60, the weak band suggesting weak or transient interaction (Fig. 5A, right panel). The reciprocal IP of CPN60 revealed that it interacts with the mature ClpP protease (I) as well as with the zymogen form (II) but not with the cytoplasmic full length PfClpP fraction (III) (Fig. 5A, left panel). This indicates that CPN60 and PfClpP interact only upon co-localization to the apicoplast and that the chaperone binds the Clp complex both before and after activation of the protease.

Typically, Clp proteolytic subunits oligomerize into heptameric rings, which consist of the core of the Clp complexes[17]. Likewise, CPN60 orthologues are part of large heptameric or tetradecameric chaperonin complexes[23]. To better understand the interaction between these large CPN and Clp complexes, we utilized structural prediction tools to explore potential binding interfaces and identify key residues for further investigation. A previous study solved the crystal structure *Plasmodium* CPN60[30]. Although in this study it was annotated as the *Plasmodium* mitochondrial HSP60, careful examination of the sequence used indicates that it is rather the structure of the apicoplast CPN60 (PF3D7_1232100). Thus, we could use it as a foundation for our predictions. As seen in its solved structure, the basic oligomeric state of CPN60 is a single heptameric ring, though a double-ring tetradecameric structure is also possible (PDB ID 7K3Z, Fig. 5B). Similarly, a solved X-ray structure of PfClpP demonstrates that it forms a tetradecamer, consisting of two heptameric rings (PDB ID 2F6I, Fig 5C)[22]. With these two solved complex structures, we set to predict how these two large complexes might interact in their 3D conformations. We

used AlphaFold3 (AF3)[31], a state-of-the-art model with a diffusion-based architecture capable of handling large protein complexes, offering improved accuracy and speed compared to AlphaFold2[32]. Due to AF3 limitations, we could only model interactions between a heptameric single ClpP ring and a heptameric CPN60 ring. Consequently, our predictions represent a partial complex rather than the full tetradecameric assemblies of both proteins. The AF3 predictions provided a model in which the PfClpP heptameric ring tilts one way, whereas the CPN60 ring tilts the other way (Fig. 5D). In this configuration it is possible for both CPN60 and ClpP complexes to form tetradecameric barrels, which interact via a stable interface (Fig. 5D and Sup. Fig. 1A). In a second possible model, both CPN60 and PfClpP rings tilt to the same direction (Sup. Fig. 1B), resulting in a conformation that does not support a tetradecamer. Based on structural considerations, the opposing-tilting PfClpP-CON60 model appears to be the more plausible conformation for the interaction between PfClpP and CPN60.

To further investigate the stability of the more favorable interaction, we performed computational alanine scanning (see methods) to identify potential interaction hotspots. As expected, the upward-tilted ClpP model exhibited significant hotspots in key residues, while the downward-tilted model did not show any meaningful interaction sites. The ClpP predicted hotspots residue were Y41, I45 and Y73 and the CPN60 hotspots residues were K243, F320 and N323 (Fig. 5E). It is important to note that these results are based on structural predictions and the hotspot residues were identified through computational alanine scanning. Additional experimental validation is required to confirm these interaction models and the proposed key residues, as well as to refine our understanding of the molecular mechanisms driving the CPN60-ClpP complex formation.

CPN60 stabilizes the active Clp complex

The AF3 model shows that both CPN60 and PfClpP complexes can form tetradecameric barrels which interact via a stable interface (Sup. Fig. 1A). This model preserves for both complexes the intra-barrel cavity necessary for the enzymatic activity of each complex independently of the other. However, immunoprecipitation showed that CPN60 also interacts with the PfClpP zymogen (Fig. 5A). We therefore used AF3 to model the PfClpP heptameric ring in its pre-activated form. In this model, the pro-domain region could only be predicted with low

confidence due to its unstructured nature and lack of homology to different ClpP orthologues in other organisms (Fig. 5F). Yet, it appears that the PfClpP pro-domain blocks the CPN60 interacting interface and therefore this model could not explain the interaction between the two complexes in the inactive state.

We therefore examined the significance of this interaction experimentally, and tested possible effects on PfClpP activity. We previously showed that PfClpP accumulates in the apicoplast as an inactive zymogen, and upon assembly of the PfClpP oligomer, it auto-cleaves itself to remove the inhibitory pro-domain and becomes activated[15]. Thus, the ratio between the inactive (band II) and active (band I) PfClpP forms is indicative of its activation state. To test the processing pattern of PfClpP upon CPN60 knockdown, we removed aTC from non-synchronous parasites and monitored proteins levels (Fig. 5G). As expected, 72 hours after knockdown induction, the parasites were dying, as indicated by diminished cellular content (represented by aldolase, Fig. 5F, lowest panel). However, at the first 48 hours and prior to phenotypic distress, a change in PfClpP processing could be observed. We detected a reduction in the levels of the active band (I) and accumulation of the inactive zymogen (II), depending on CPN60 levels (Fig. 5G). This significant shift in the ratio of active: inactive PfClpP could be quantified (Fig. 5H), suggesting that the interaction between CPN60 and PfClpP is essential for PfClpP auto-processing and complex stability.

Exploiting the apicoplast chaperonin system as an antimalarial target

Inhibiting protein synthesis in the apicoplast is a clinically approved drug target, as indicated by the antimalarial effect of doxycycline. Nevertheless, such treatment directly affects only a fraction of the total apicoplast proteome. Although largely unexplored, post-translational regulation in the organelle is no less critical and likewise can prove druggable. In this regard, the essentiality of CPN60 described here supports its viability as a potential antimalarial target.

To test this, we took advantage of a series of bacterial inhibitors designed to target the prokaryotic CPN60 orthologue, GroEL. As far as we are aware, chaperonin inhibitors have never been explored against *Plasmodium*. Thus, we conducted a pilot study to test the efficacy of a panel of phenylbenzoxazole (PBZ) analogues. PBZ compounds were previously shown to bind and inhibit the activity of GroEL in *E.* Coli, inducing a separation and a twist of the two rings that decoupled their inter-ring

allosteric signaling, thereby blocking the folding cycle[33]. Detailed cryoEM structures showed that the PBZ analogue PBZ1587 binds at the GroEL ring-ring interface[34]. Moreover, it was shown that mutations of key residues within the interface binding site render GroEL resistant both *in vitro* and in *E. coli*, demonstrating on-target antibacterial effects, and a validated tool for other studies. We therefore hypothesized that PBZ analogues have the potential to bind one of the *Plasmodial* chaperonin systems, either the apicoplast CPN60, the mitochondrial HSP60, or both.

To test the antimalarial potential of the PBZ inhibitors, we incubated parasites with serial dilutions of each (50 μM to 50 nM) and monitored growth after 72 or 96 hours to calculate the inhibitor half-maximal effective concentrations (EC50) (Fig. 6 and Table 1). Although some inhibitors showed moderate activity against *P. falciparum* growth (1134, 1135, 1259), others produced an EC50 at a single-digit micromolar range (1001, 1064, 1133, 1207, 1221) or lower (1587), demonstrating a potent anti-*Plasmodial* activity (Figure 6 and Table 1).

Next, we wanted to assess whether compound efficacies result from compromising apicoplast function, putatively through inhibiting CPN60, through the addition of IPP to bypass dysfunction. We incubated the parasites with a fixed inhibitor concentration of 12.5 μM (roughly 2-3X folds of most EC50s), and monitored their growth over 96 hours. While IPP did not affect growth of untreated parasites, it fully restores viability of chloramphenicol-treated parasites, which inhibit apicoplast translation (Fig. 7A). However, the toxic effect of the PBZ inhibitors could not be restored by IPP, suggesting that (1) the 12.5 μM test concentration may have been too high above inhibitor EC50 values, making rescue unfeasible (i.e. PBZ1587), or (2) inhibitors could be functioning against additional targets, the most likely candidate being mitochondrial CPN60. However, the moderately potent inhibitor PBZ1214 (EC50 = 9.6-12.5 μM) presented an intriguing result as IPP treatment sensitized parasites to the inhibitor (Fig. 7B & C). The reason(s) for IPP sensitization of PBZ1214 is unclear at present and will require further investigation.

Discussion

Chaperonins (CPN60/ HSP60) function biochemically as ATP-dependent molecular chaperones, working in concert with other chaperones and co-chaperones to facilitate protein folding and maintain proteostasis. Chaperonins are originally prokaryotic proteins and are essential in almost all bacteria, where they are known as GroEL, as well as in all endosymbiotic organelles[23]. Indeed, an HSP60 homolog is found in the mitochondria of almost all eukaryotes, including human and *Plasmodium*, although the latter has not been well characterized. Another GroEL homolog is found in chloroplasts[35] (an essential Rubisco binding subunit) as well as in related non-photosynthetic plastids, including the apicoplast organelle of *Apicomplexan* parasites. Aside from bioinformatic predictions, prior works in *Toxoplasma gondii* reported on the expression and localization of an apicoplast CPN60[26,36]. We previously reported and used CPN60 as an apicoplast localization marker[15]. However, so far, the physiological or molecular functions of the apicoplast CPN60 remained to be resolved.

In this work, we addressed these questions by undertaking genetic and cellular approaches to investigate organellar functions of the apicoplast CPN60. To do so, we used CRISPR-mediated genetic engineering to modify the *cpn60* genetic locus to introduce a V5 peptide tag, followed by the tetR-Dozi system that enables conditional knockdown of *Plasmodium* proteins (Fig. 1). Despite the fact that GroEL/ HSP60s are considered housekeeping genes, we found that expression of *Plasmodium* CPN60 is not consistent or uniform throughout the parasite's intraerythrocytic life cycle, but rather peaks at the last hours (Fig. 1C and 1E). This expression profile correlates with the timing of apicoplast development, elongation, branching and division[37], supporting a potential function for CPN60 in organelle biogenesis. We also compared protein levels with CPN60 transcripts[38] and found that the latter peak at 24 hours post invasion (Fig. 1D). The difference in timing between peak levels of CPN60 mRNA and protein may be partly explained by a kinetic steady state of transcription and translation. However, this roughly 20 hours gap is quite extended and may also reflect additional posttranslational mechanisms in the apicoplast affecting CPN60 proteostasis. With this in mind, we also observed an unexpected third lower band for CPN60, appearing in the last hours (Fig. 1C). The upper two bands, a cytoplasmic fraction with a transit peptide (TP), and a second lower band of

the main apicoplast-localized fraction after TP removal, are expected and typical for apicoplast proteins. The third lowest band putatively represents an unknown posttranslational modification, the significance of which remains to be resolved.

Knock down of CPN60 levels by removing the tetracycline analogue aTC proved extremely efficient, diminishing CPN60 to less than 10% within the first 48 hours (Fig. 2A and 2B). Consequently, parasites died within the first 48 hours, a phenotype that could be completely rescued by IPP addition, demonstrating an apicoplast-restricted function. (Fig. 2C and 2D). Interestingly, removing aTC from early-ring-stage synchronous parasites resulted in their immediate-death within the first replication cycle. This phenotype is different and faster than the more typical apicoplast-delayed cell death, observed in parasites treated with apicoplast-targeting antibiotics[29]. This kinetics is more similar to the effect of drugs blocking isoprenoids synthesis, which also target the apicoplast but kill within one replication cycle[11,39]. Thus, CPN60 knockdown adds to growing evidence of immediate cell death resulting from inhibition of apicoplast biogenesis[40,41], underlying its potential as a drug target.

In bacteria and plant chloroplasts, CPN60 is critical for heat shock (HS) response. In the case of *Plasmodium*, the parasite copes and responds to periodic fever episodes during infection of the human host[42,43]. Because its ER repertoire of molecular chaperones is limited[44], it would have been intriguing if the apicoplast chaperonin complex is somehow complementing the stress response mechanism. Indeed, a recent large-scale forward-genetic screen suggested a link between the apicoplast and fever-survival[45]. However, during recovery after HS, CPN60 levels remained constant (Fig. 3A and 3B). Because complete removal of aTC leads to parasite death regardless of temperature, we titrated aTC concentrations to reach low CPN60 levels that support 50% growth. To do that, we determined the EC50 of aTC in CPN60 parasites under normal conditions and following heat exposure, and demonstrated that HS does not sensitize the parasite to perturbations in CPN60 levels (Fig. 3C and 3D). This also provided us with a tool of reducing aTC to the point where CPN60 levels are 50% reduced (4-8 nM), not unlike a hippomorphic allele with a partial loss of function (Fig. 3E and 3F). Using this system enabled us to determine unequivocally that unlike CPN60 in most organisms, the *Plasmodium* homolog is not involved in heat shock response.

We next investigated potential functions of CPN60 in organellar protein quality control pathways. In plant chloroplasts, the Clp (caseinolytic protease) system is the primary machinery for protein degradation in the plastid stroma[19]. Likewise, in the apicoplast of *P. falciparum*, Clp proteins form an organellar degradation machinery that is independent of the cytoplasmic proteasome[15,22]. We therefore investigated a potential chaperonin-Clp interaction by co-expressing a tagged copy of PfClpP (Fig. 4). Previous findings suggested that PfClpP is a potent protease and its overexpression may be toxic to the parasites. Likewise, bacteriocidic effects of the ClpP activators ADEP demonstrate that enhanced Clp activity is toxic[46]. We therefore used a protease dead variant that was shown to be inactive, but can be expressed and incorporated into functional multi-subunit complexes without negative consequences[15]. Indeed, expression of $ClpP^{DEAD}$ variant showed co-localization with CPN60 in the apicoplast, and had no effect on the EC50 of aTC in normal or febrile temperatures (Fig. 4).

Next, we used co-immunoprecipitation to demonstrate that PfClpP and CPN60 physically bind each other (Fig. 5). In previous studies[14,15], we showed that a tightly synchronized sequence of events determines the activity of the Clp complex; PfClpP zymogen subunits oligomerize once localize to the organelle, inhibitory pro-domain is removed by trans-autocatalysis and only then, the Clp chaperone PfClpC binds the proteolytic ring, a binding that is essential for complex stability. In this co-IP experiment, we found that CPN60 binds not only the active fraction of PfClpP (like PfClpC), but also the inactive zymogen before the removal of the inhibitory pro-domain. Using AF3 predictions based on solved ring structures, showed that PfClpP and CPN60 oligomerize and interact via heptameric rings. This model predicted that the PfClpP ring is tilting one way, while the CPN60 heptameric ring is tilting the other direction, thus forming a configuration that would allow for both PfClpP and CPN60 tetradecamers to form and stabilize (Fig. 5 and Sup. Fig. 1). We also modeled PfClpP oligomeric ring in its pre-activated state, however the model could not explain how the CPN60 ring would stably interact with the PfClpP zymogen oligomer.

This intrigued us to examine the biochemical significance of the dynamic interaction between the chaperonin and both states of the PfClpP complex. Interestingly, we discovered that upon CPN60 removal, active PfClpP levels decline, while PfClpP zymogen levels increase. Until this point, we operated under the hypothesis that,

similar to chaperonin orthologs in other organisms, the apicoplast CPN60 acts as a "conformational editor" to assist in organellar folding processes. These unexpected results showed that at least part of its activity is to stabilize and activate the Clp complex, thus supporting organellar degradation processes. Based on these results, we propose a working model in which the interdependence between two complexes with opposing functions, facilitates a balanced proteostasis in the apicoplast (Fig. 8).

Over years of research, chaperonins have been identified as potential targets for the development of novel agents affecting their activity. Many of those have implications for new-generation antibiotics, cancer and neurodegeneration treatment, as well as the development of diagnostic biomarkers[23,47–49]. Nevertheless, the potential of mitochondrial and/or apicoplast CPN60 as viable targets for antimalarial development have not been investigated. From an evolutionary point of view, and despite being quite different in sequence, the apicoplast CPN60 is closer to its bacterial orthologue GroEL than to mitochondrial chaperonins found in most eukaryotes (See Sup. Fig. 2 for sequence alignment). Here we tested the antimalarial activity of a small panel of phenylbenzoxazole (PBZ) compounds that were originally identified as inhibitors of the *E. coli* GroEL/ES chaperonin system[33]. These inhibitors exhibited antibiotic effects from the low-μM to mid-nM range against a panel of Gram-positive and Gram-negative bacteria[47], mycobacteria[50] and even *Trypanosoma* parasites[51], highlighting the versatility of targeting chaperonins.

Within the group of PBZ anti-GroEL inhibitors tested here, we found compounds with antimalarial effect at the low and sub-micromolar range (Fig. 6, Table 1). However, their cytotoxic effects were not reversed with IPP supplementation, suggesting additional targets beyond the apicoplast CPN60 (Fig. 7). This lack of specificity could be explained by the presence of two other chaperonin systems in the parasite in addition to the on one in the apicoplast. One of them is the mitochondrial HSP60, that like the apicoplast CPN60 belongs to the Type I chaperonins which are common to all bacteria and endosymbiotic organelles in humans, plants and parasites.

Another is the type II chaperonin, which is found in archaebacterial cytoplasm (thermosome) and eukaryotic cytosol (CCT/TRiC)[52]. Based on recognized and separated evolutionary lines, the TriC system is generally poorly characterized comparing to the type I HSP60. Uncharacteristically, the CCT/TRiC system in *Plasmodium* has been investigated more than its type I variant, and shown to be a

valid drug target[53–55]. Whether it is also targeted by PBZ inhibitors, or can explain the IPP toxicity that is associated with some of them, remains to be investigated.

To conclude, by investigating the relationship between the *Plasmodium* Chaperonin and Clp complexes, we revealed two opposing mechanisms that interact to balance proteostasis in the apicoplast. These detailed cellular, biochemical and bioinformatic analyses shed light on how excessive degradation is avoided when folding is compromised, to regain steady state (Fig. 8). We further provide a foundation for systematic evaluation of these mechanisms and the potential of targeting CPN60 as an antimalarial strategy. Future studies focusing on their bacterial evolutionary origins could use existing antibacterial compounds to streamline drug discovery.

Materials & Methods

Plasmids construction

Genomic DNA was isolated from *P. falciparum* using NucleoSpin blood kit (Machery-Nagel). For the generation of the CPN60$^{V5\text{-}apt}$; conditional mutant, 500 bps from the C-term and 3'UTR from the of *cpn60* gene (Pf3D7_1232100) were amplified from genomic DNA using primers P1+P2 and P3+P4, respectively. The two products were conjugated together using overlap extension PCR and inserted as one piece into pMG74-tetR-Dozi vector[27]. For expression of a C-term CPN60 guide RNA, oligos P8+P9 were annealed and inserted into pUF1-Cas9-guide. Primer P7 was used in combination with primer P6 or P4 to test for accurate integration in the parasite genome following transfections. Evaluating aptamer repeats number was done using primers P5+P6.

For the generation of ClpP^{DEAD} parasites, we transfected parasites with the puc-HSP110-ClpP$^{DEAD\text{-}Ty}$ plasmid which we used previously to study ClpP processing and activation[15]. It encodes the entire Open Reading Frame of ClpP (PF3D7_0307400), mutated in three residues: Ser264Ala, Glu308Arg and Arg285Glu, following by a triple Ty tag. Expression is driven under the *Pfhsp110c* gene (PF3D7_0708800). Briefly, the HSP110 expression system comprises of a repair plasmid that contains homology sequences from the *Pfhsp110c* gene. The repair sequences include the last 429 bp (not including the stop codon) from the *Pfhsp110c* gene, followed by a 2A skip peptide, ClpP$^{DEAD\text{-}Ty}$ sequence and the first 400 bps from *Pfhsp110c* 3'UTR. For expression of a *Pfhsp110c* guide RNA, oligos P10+P11 are expressed from pUF1-Cas9-guide. Primers P12 and P13 were used to test for accurate integration in the parasite following transfections.

All constructs utilized in this study were confirmed by Sanger sequencing. PCR products were inserted into the respective plasmids using In-Fusion Snap assembly Master mix (Takara). All restriction enzymes used in this study were purchased from New England Biolabs. Oligonucleotides used in this study are summarized in Table 2.

Cell culture and transfections

Parasites were cultured in RPMI medium supplemented with Albumax I (Gibco) and transfected as described earlier[56–58]. Synchronization of cultures were achieved by intermittent sorbitol and Percoll treatments. To generate CPN60$^{V5\text{-}apt}$ parasites, a mix of two plasmids was transfected into NF54 *wildtype* parasites in the presence of 0.5

mM anhydrotetracycline (aTC, Cayman Chemicals). The plasmid mix contained 40 μg of pUF1-Cas9-guide expressing the CPN60 guide, and 20 μg of pMG74-based donor plasmid with CPN60 homology regions, linearized by EcoRV. Drug pressure was applied 48 hours post transfection using 2.5 μg/ml Blasticidin (BSD, Sigma). For each transfection, at least 2 clones (A4 and F11) were isolated via limiting dilutions and used in all subsequent experiments.

To generate CPN60$^{V5\text{-}apt}$; ClpP^{DEAD} parasites, a mix of two plasmids was transfected into CPN60$^{V5\text{-}apt}$ parasites. The mix contained 2 plasmids; 40 μg of pUF1-Cas9-*Pfhsp110c*-guide and 40 μg of the marker-less repair plasmid puc57-HSP110-ClpP^{DEAD}. Drug pressure was applied 48 hours post transfection, using 1 μM DSM1 (BEI Resources), selecting for Cas9 expression. DSM1 was removed from the culturing media once parasites clones were isolated by limiting dilution. For each transfection, at least 2 clones (D12 and H10) were isolated via limiting dilutions and used in all subsequent experiments.

Growth assays

For CPN60 knockdown assays, asynchronous parasite cultures were washed 8 times and incubated without aTC. Throughout the course of the experiment, parasites were sub-cultured to maintain parasitemia between 1-5% and parasitemia was monitored every 24 hours via flow cytometry. The parasitemia levels were determined in comparison to negative control (uninfected RBCs). Cumulative parasitemia at each time point was back calculated based on actual parasitemia multiplied by the relevant dilution factors. Parasitemia in the presence of aTC at the end of each experiment was set as the highest relative parasitemia and was used to normalize parasites growth. Normalized data from technical replicates were analyzed and fit to an exponential growth curve using Prism (GraphPad Software, Inc.) All experiments shown are representative of at least three biological replicates. For IPP rescue, media was supplemented with 200 μM IPP (Isoprenoids LC).

Flow cytometry

Aliquots of parasite cultures (5 μl) were stained with 8 μM Hoechst (ThermoFisher Scientific) in PBS. The fluorescence profiles of infected erythrocytes were measured and analyzed by flow cytometry on a CytoFlex S (Beckman Coulter). The parasitemia data were analyzed and presented using Prism (GraphPad Software, Inc.).

Recovery after heat shock

To induce heat shock response, parasites were incubated at 40ºC for 24 hours and then allowed to recover at 37ºC to mimic the characteristic malarial fever episodes. Growth of recovered parasites was monitored over the next following days using flow cytometry and protein samples were isolated as described below. When CPN60 levels were to be manipulated, aTC was first washed away, and parasites were subjected to heat shock 24 hours later to allow protein levels to drop.

Half-maximal effective concentration (EC50)

To generate an EC50 curve for aTC, asynchronous cultures of $CPN60^{V5\text{-}apt}$ or $CPN60^{V5\text{-}apt}$; $ClpP^{DEAD\text{-}Ty}$ parasites were washed 8 times and then seeded at 0.5% parasitemia in a 96 well plate with varying concentrations of aTC. To measure aTC EC50 after recovery from heat shock, parasites were similarly treated, incubated for 24 hours at 40ºC, and then returned to 37ºC for the rest of the experiment. To generate EC50 curves for HSP60 inhibitors, NF54 *wildtype* parasites were seeded at 0.5% parasitemia in a 96 well plate with varying concentrations of each compound. In all cases parasitemia was measured after 72- and 96-hours using flow cytometry. Data were fit to a dose-response equation using Prism (GraphPad Software, Inc.).

Inhouse anti-Ty tag monoclonal antibody purification

The hybridoma BB2 clone cell line (a kind gift from Boris Striepen) was adapted to serum-free medium. 500 ml spent medium of the hybridoma clone containing mAbs was collected, concentrated and purified by HiTrap™ Protein G HP antibody purification 1 ml column (Cytiva) operated by peristaltic pump, as per manufacturer protocol. The bound antibody was eluted using 10 ml 0.1 M Glycine-HCl buffer, pH 2.7 for ten minutes, and then neutralized with 1M Tris-HCl, pH 9.2 buffer. The protein content was determined and adjusted to 1 mg/ml.

Immunoprecipitation

Co-Immunoprecipitation (Co-IP) protocols were performed using anti-V5 antibody ($CPN60^{V5\text{-}apt}$) or anti-Ty antibody ($ClpP^{DEAD\text{-}Ty}$). Pellets from $4x10^8$ parasites were isolated using cold saponin and were lysed and sonicated in Extraction Buffer (40 mM Tris HCl pH 7.6, 75 mM KCl, and 1 mM EDTA, 15% glycerol) supplemented with HALT protease inhibitor (Thermo). 10% of the sample was kept for later analysis (input sample). Rabbit anti-V5 (Cell Signaling, D3H8Q) or anti-Ty, BB2 (inhouse purification) antibodies were crosslinked to Dynabeads protein G beads (Invitrogen) by incubating

with 5 mM BS3 crosslinker (CovaChem) for 30 minutes. Quenching of crosslinker was performed using 1 M Tris HCl (pH 7.5) for 30 minutes and then washing with 1.2M Glycine HCl (pH 2.5) to remove excess unbound antibody. Antibody-conjugated beads were then washed 3 times with PBS and incubated with the supernatant at 4°C. Washes were performed using a magnetic rack (Life Technologies). Samples were run on SDS-page and blotted with anti-V5 or anti-Ty antibodies.

Western blot

Western blots were performed as described previously[15]. Briefly, parasites were collected and host red blood cells were permeabilized selectively by treatment with ice-cold 0.04% saponin in PBS for 15 min, followed by a wash in ice-cold PBS. Cells were lysed using RIPA buffer, sonicated, and cleared by centrifugation at 4oC. The antibodies used in this study were mouse anti-Ty, BB2 (inhouse purification), rabbit anti-V5, D3H8Q (Cell Signaling, 1:3000), mouse anti-V5, E9H80 (Cell Signaling, 1:3000), rabbit anti-aldolase ab207494 (abcam, 1:3000). The secondary antibodies that were used are IRDye 680CW goat anti-rabbit IgG and IRDye 800CW goat anti-mouse IgG (LICOR Biosciences, 1:20,000). The Western blot images and quantifications were processed and analyzed using the Odyssey infrared imaging system software (LICOR Biosciences). Three biological replicates were used for quantification of expression levels (Fig.1), HS response (Fig.3), partial knockdown (Fig.3), and ratio of ClpP processing (Fig.6) using Prism (GraphPad Software, Inc.).

Microscopy and image processing

For IFA, cells were fixed using a mix of 4% paraformaldehyde and 0.015% glutaraldehyde and permeabilized using 0.1% Triton-X100. Primary antibodies used are mouse anti-Ty1, BB2 (Invitrogen, 1:100), and rabbit anti-V5, D3H8Q (Cell Signaling, 1:100). Secondary antibodies used are Alexa Fluor 488 and Alexa Fluor 546 (Life Technologies, 1:100). Cells were mounted on Fluoroshield with DAPI (Sigma). The imaging was performed using Airyscan2 LSM980 confocal microscope equipped with 62x/1.4NA objective. Images were collected as Z-stack, and displayed as maximum intensity projection. Image processing, analysis and display were performed using Zeiss ZEN 3.7 Software. Adjustments of brightness and contrast were made for display purposes. Blood smears were imaged using an upright Eclipse E200 Microscope (Nikon), equipped with x100 oil objective Type NVH, and captured using a

digital Sight 1000 microscope camera and NIS-Elements Software (Nikon). Figures for this manuscript were generated using BioRender.com.

AF3 structure prediction

The inputs are protein and peptide sequence. All different versions were run with random seed 2 or 1. Runs was done on alphafold server from GitHub (https://alphafoldserver.com/). Structural Visualization was done using the PyMOL Molecular Graphics System (Version 2.4.0) and UCSF ChimeraX (Version 1.4).

Alanine scanning

Robetta computational alanine scanning was applied to define the critical interface residues, as implemented in http://robetta.org. Detailed protocol was described by Kortemme *et al*[59].

Data Availability

All of the data described are included in the manuscript and Figures.

Acknowledgements

We thank Boris Striepen for the BB2 hybridoma cell line; Florentin lab members for critical reading and comments on the manuscript; Yael Feinstein-Rotkopf at the Imaging Core Facility at the Faculty of Medicine, En Kerem; VEuPathDB and PlasmoDB for scientific, academic and community support. This work was supported by grants from the Israel Science Foundation [400/22 (personal grant) and 2786/22 (equipment grant)] and HUJI start-up funds to AF. AT is supported by a PhD scholarship from Science Training Encouraging Peace (STEP). AF is supported by the Abisch-Frenkel Faculty Development Lectureship. AF, AT, MS and YR acknowledge support by The Kuvin Center for the Study of Infectious and Tropical Diseases.

Figures

Figure 1

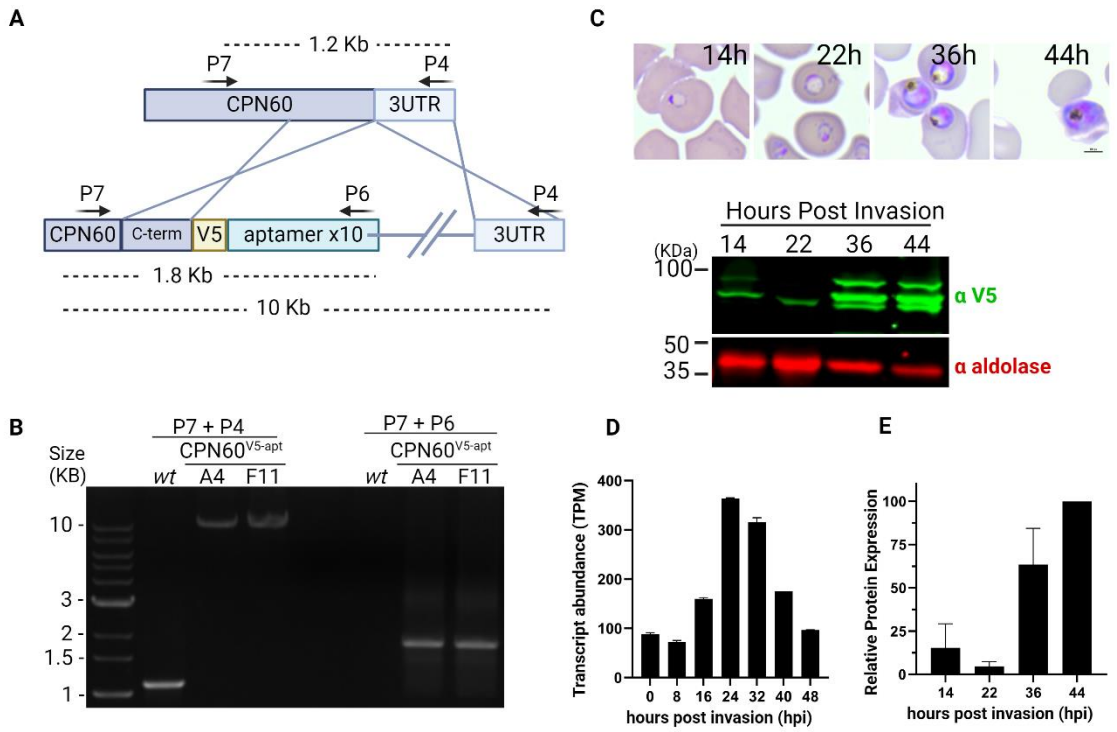

Figure 1. Generation and characterization of transgenic CPN60$^{V5\text{-}apt}$ parasites. A. Schematic representation of CRISPR-mediated homologues recombination through CPN60 homology regions enabling the integration of the V5 tag and the tetR-Dozi system. **B.** PCR amplification of genomic DNA isolated from CPN60 transfected parasites. Primers used are depicted in A and in Table 2. Primers are integration specific and thus can amplify 1.6 KB (P7+P6) and 11 KB (P7+P4) products only if integration occurs at the desired genomic locus. **C**. Western blot depicting expression profile of tagged CPN60 throughout parasite life cycle using an anti-V5 antibody. Blood smears above demonstrate parasites' developmental stage at the time of protein extraction. **D.** Quantifications of CPN60 transcript[38] (TPM; Transcripts Per Million). **E.** Densitometric analysis of protein bands from Western blot in C.

Figure 2

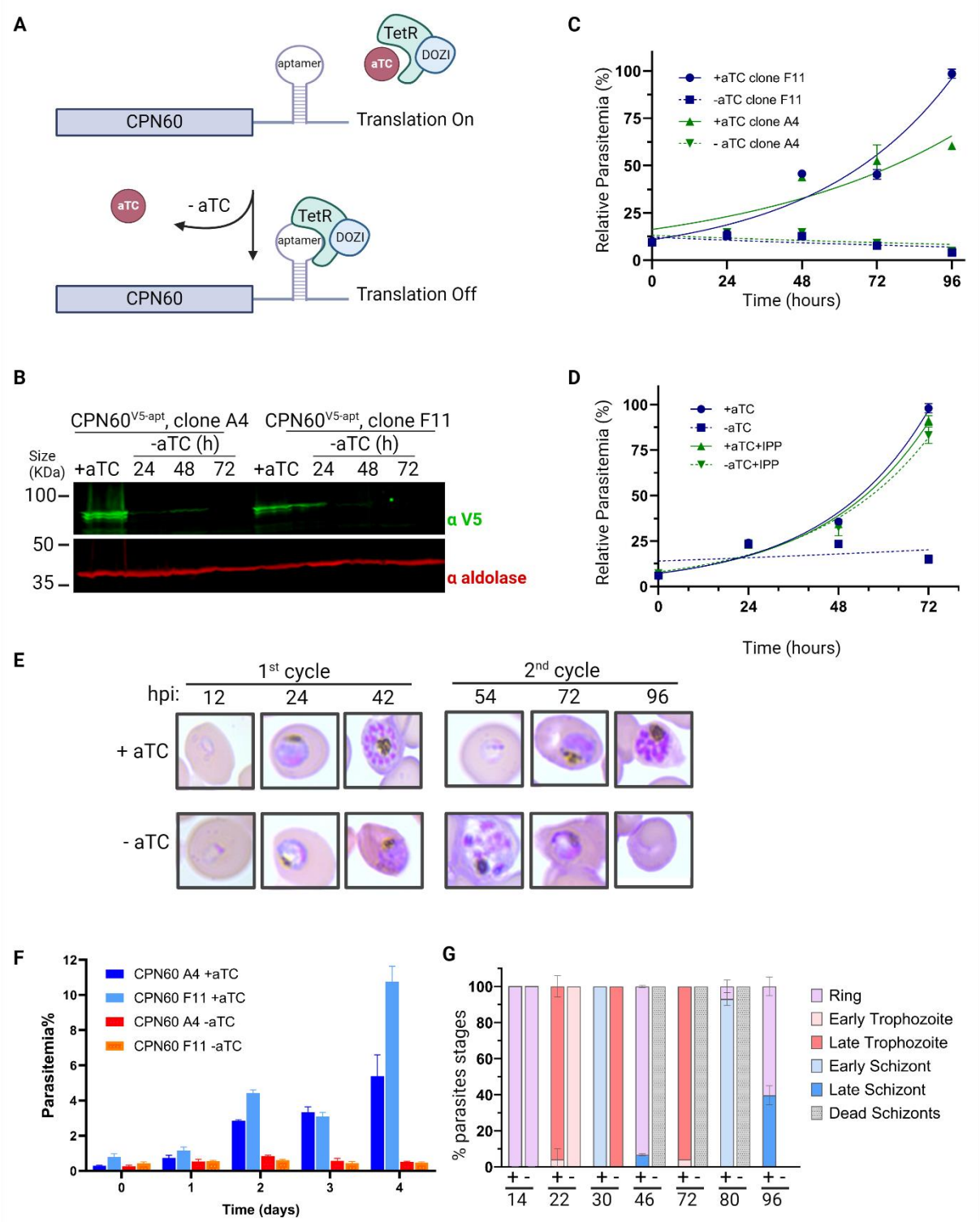

Figure 2. CPN60 is essential for parasite's viability due to its apicoplast function. **A.** Schematic representation of the tetR-Dozi system, which enables protein knockdown upon removal of the tetracycline analogue aTC. **B.** Western blots depicting the expression of the tagged CPN60 using an anti-V5 antibody following knockdown induction. A significant reduction in protein levels is already observed after 24 hours,

and falls below detection 72 hours after aTC removal. **C.** Growth curve of CPN60$^{V5\text{-}apt}$ parasites. Independent CPN60$^{V5\text{-}apt}$ clones A4 and F11 were grown with or without 0.5 mM aTC, and parasitemia was monitored every 24 h over two cycles via flow cytometry. The 100% of growth represents the highest value of calculated parasitemia (final parasitemia in the presence of aTC). Normalized data are represented as mean ± SEM for three technical replicates. **D.** Growth curve of CPN60$^{V5\text{-}apt}$ parasites, clone A4, supplemented with 200 μM IPP. The 100% of growth represents the highest value of calculated parasitemia (final parasitemia in the presence of aTC). Normalized data are represented as mean ± SEM for three technical replicates. **E.** CPN60$^{V5\text{-}apt}$ parasites were synchronized by incubation with 5% sorbitol followed by Percoll-mediated schizont-enrichment the following day. Synched parasites were washed 8 times and then incubated with or without aTC. Giemsa-stained blood smears were imaged using an upright Eclipse E200 Microscope. **F.** Growth rates of synchronous CPN60$^{V5\text{-}apt}$ parasites. Clones A4 and F11 were grown with or without 0.5 mM aTC, and parasitemia was monitored every 24 h over two cycles via flow cytometry. Data are represented in columns as mean ± SEM for three technical replicates. **G.** Blood smears of synched CPN60$^{V5\text{-}apt}$ parasites with or without aTC were analyzed for specific parasites developmental stages. Minus aTC parasites demonstrate a delayed trophozoite stage already on the first replication cycle, fail to egress, and die during schizogony.

Figure 3

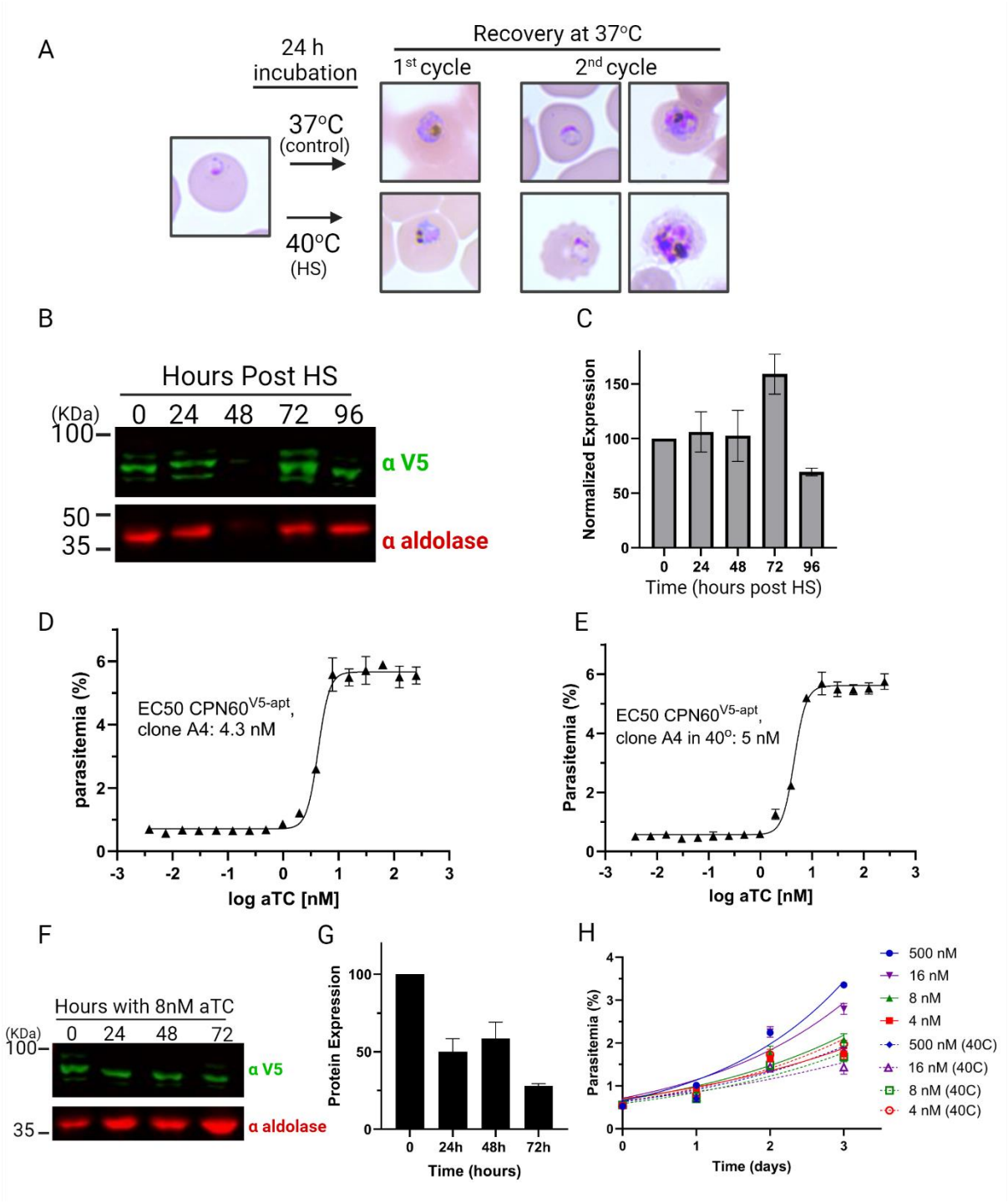

Figure 3: **CPN60 is not involved in Heat Shock response**. **A.** Workflow of HS experiments and representative blood smears. Parasites are subjected to HS at 40ºC for 24 hours and then allowed to recover at normal temperature (37ºC). **B.** Parasites were subjected to HS and recovery as depicted in (A). Cellular lysates were extracted every 24 hours over a span of four days and subjected to Western blot analysis using an anti-V5 antibody to follow tagged CPN60 levels. **C.** Quantification of CPN60 levels

post-heat shock (shown in B) demonstrate no significant increase in protein levels. **D.** To calculate EC50 of aTC, CPN60$^{V5\text{-}apt}$ parasites were thoroughly washed to remove aTC, and then incubated in serial aTC dilutions in a 96-well plate. Parasitemia was measured after 4 days using flow cytometry, showing an EC50 of 4.3 nM. Data are fit to a dose-response equation and are represented as mean ± SEM. One representative experiment out of three is shown. **E**. aTC EC50 in CPN60$^{V5\text{-}apt}$ during HS. Parasites were washed and treated as in (D). The plate was then transferred to 40ºC for 24 hours and then allowed to recover at 37ºC . Parasitemia was measured after 4 days using flow cytometry, showing an EC50 of 5 nM. Data are fit to a dose-response equation and are represented as mean ± SEM. One representative experiment out of three is shown. **F**. Parasites were thoroughly washed and then incubated with 8 nM aTC (2X EC50). Parasites lysates were obtained every 24 hours and subjected to western blot analyses by being probed with antibodies against V5 (green) and aldolase (loading control, red). The protein marker sizes that co-migrated with the probed protein are shown on the left. **G.** Densitometric analysis of protein bands from Western blot in (F) indicating 50% drop in CPN60 expression. **H.** CPN60$^{V5\text{-}apt}$ parasites were washed and incubated with different aTC concentrations (8 nM, 4 nM, 16 nM and 500 nM), subjected to HS and then allowed to grow at 37ºC for three days, while being measured daily by flow cytometry.

Figure 4

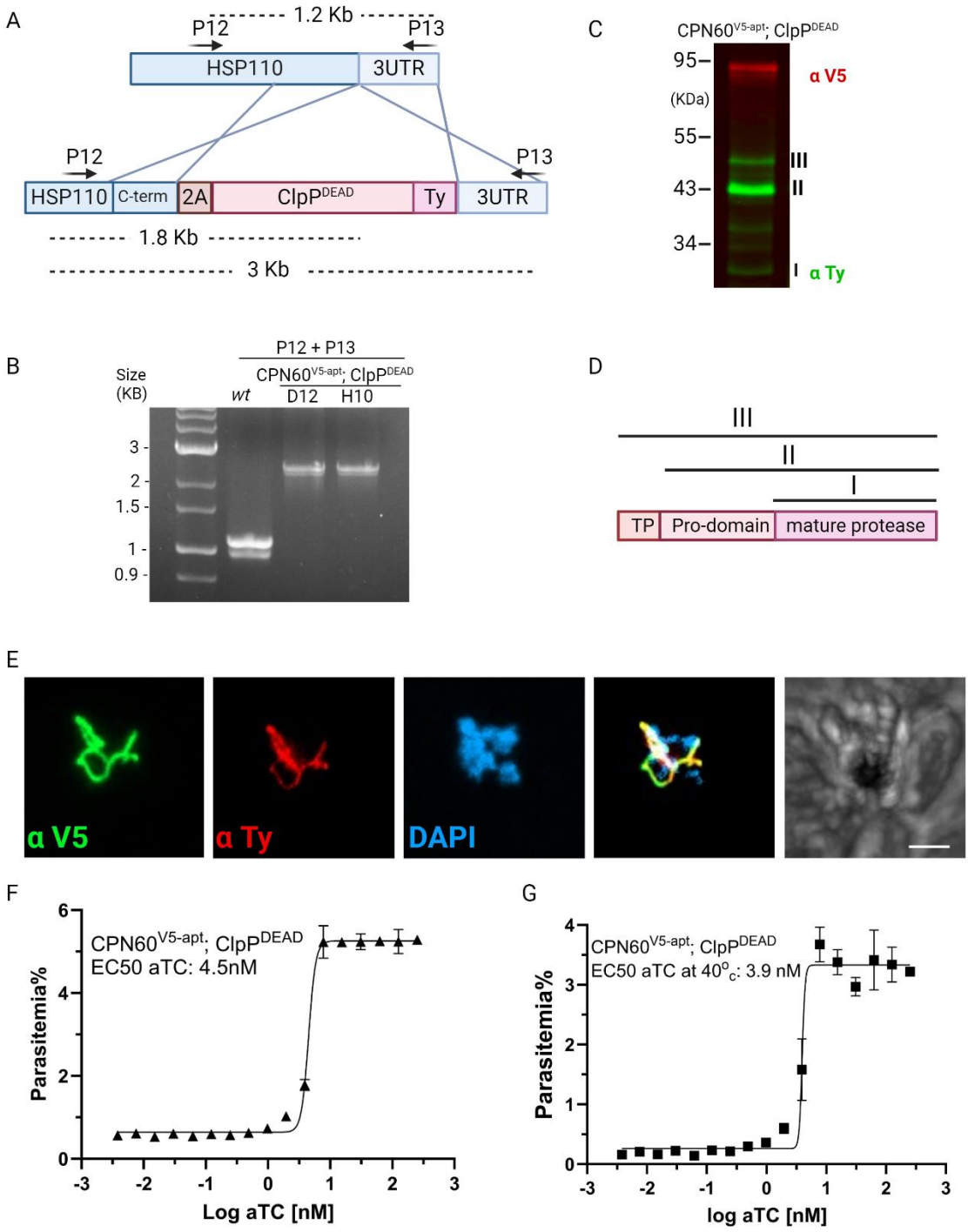

Figure 4: Co-expression and co-localization of CPN60 and PfClpP. A. A diagram depicting integration of a transgenic inactive PfClpP with a point mutation in the proteolytic active site (S264A) and a C-terminal Ty tag. CRISPR-mediated integration into the parasite's genome under the endogenous *hsp110* promoter enables constant and moderate expression. **B.** Genotyping by PCR to confirm ClpP$^{DEAD\text{-}Ty}$ integration at the *hsp110* locus. Genomic DNA was purified from transfected isolated parasites

clones (D12 and H10), and primers P12 and P13 were used to specifically amplify the integrated region. A shift of 1000 bp corresponds to the integration of $ClpP^{DEAD\text{-}Ty}$. **C.** Western blot analysis of lysates from $CPN60^{V5\text{-}apt}$; $ClpP^{DEAD\text{-}Ty}$ parasite line, probed with antibodies against V5 (red) against TY (green) showing the co-expression of the two proteins. **D.** Schematic representation of the PfClpP processing as seen in C.: Full length cytoplasmic PfClpP with the transit peptide (TP, III), apicoplast-localized fraction after TP removal (II) and mature PfClpP after proteolytic cleavage of the pro-domain (I). **E.** Immunofluorescence microscopy of $CPN60^{V5\text{-}apt}$; $ClpP^{DEAD\text{-}Ty}$. Z stack images processed as Maximum Intensity show from left to right: anti-V5 (CPN60, green), anti-ty ($ClpP^{DEAD\text{-}Ty}$, red) and DAPI (parasite nucleus, blue), along with merged fluorescentt channels, and phase contrast. Scale bar is 5 μM. **F.** EC50 of aTC in $CPN60^{V5\text{-}apt}$; $ClpP^{DEAD\text{-}Ty}$ parasite in 37ºC (**F**) and following 24 hours incubation at 40ºC (**G**). Parasites were washed to remove aTC, and then incubated in serial aTC dilutions in a 96-well plate. Parasitemia was measured after 4 days using flow cytometry, showing comparable EC50s of 4.5 nM (F) and 3.9 nM (G). Data are fit to a dose-response equation and are represented as mean ± SEM. One representative experiment out of three is shown.

Figure 5

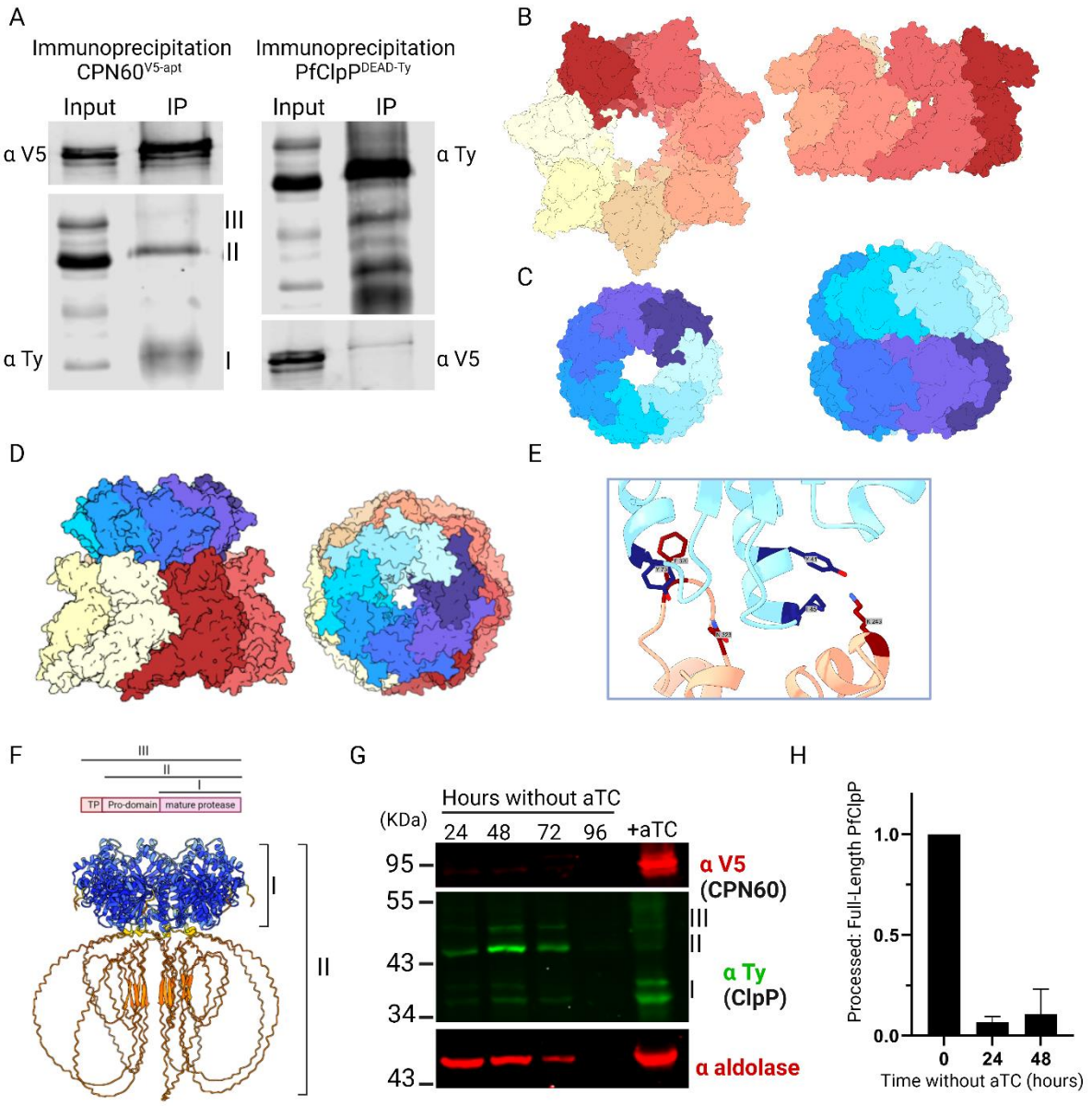

Figure 5. CPN60 binds and stabilizes the Clp complex. A. Co-IP of CPN60$^{V5\text{-}apt}$ and ClpP$^{DEAD\text{-}Ty}$. Parasites were isolated and sonicated, and extracts were incubated with either anti-V5 antibody-conjugated beads (for CPN60 pulldown, left) or anti-Ty antibody-conjugated beads (for PfClpP pulldown, right). Input and IP samples were loaded on SDS-page and blotted with anti-Ty and anti-V5 antibodies. **B.** The X-ray structure of apicoplast CPN60 (PDB ID: 7K3Z)[30]. The different chains are highlighted in different yellow and red colors, revealing the heptameric arrangement of the CPN60 ring. On the left is a top view, and on the right is a side view. **C.** The X-ray structure of PfClpP (PDB ID: 2F6I)[22]. The different chains are highlighted in different blue shades, revealing the heptameric arrangement of the PfClpP ring. On the left is a top

view, and on the right is a side view. **D.** AF3 structure prediction of the interaction between the two heptameric rings of CPN60 and PfClpP. The PfClpP ring is shown tilting upward, binding to the upper side of CPN60. PfClpP is depicted in blue and teal shades, while CPN60 is coloured in red and beige. On the left is a side view, and on the right is a top view. **E.** Alanine scanning predicting hotspot residues in the interaction between PfClpP and CPN60. CPN60 is shown in salmon, and PfClpP in light blue. Hotspot residues predicted by Alanine scanning are highlighted in dark blue for PfClpP and dark red for CPN60, indicating key interaction residues. **F.** Structure prediction of the oligomerized PfClpP zymogen coloured by confidence levels according to pLDDT scores. High-confidence regions are shown in blue, while low-confidence regions are depicted in red, indicating the varying reliability of the predicted structure. The upper panel shows schematic representation of PfClpP posttranslational processing. **G.** $CPN60^{V5\text{-}apt}$; $ClpP^{DEAD\text{-}Ty}$ parasites were incubated without aTC for 24 h, and lysates were extracted and subjected to Western blot analysis using antibodies against V5 (CPN60, red), Ty ($ClpP^{DEAD\text{-}Ty}$ parasite, green) and aldolase (red, following membrane stripping). CPN60 knockdown results in the disappearance of the processed form of PfClpP (I) and accumulation of the inactive zymogen (II). **H.** Densitometric analysis of PfClpP protein bands from Western blot in C indicate a significant reduction in PfClpP processing suggesting that the interaction with CPN60 is essential for Clp complex activity.

Fig. 6

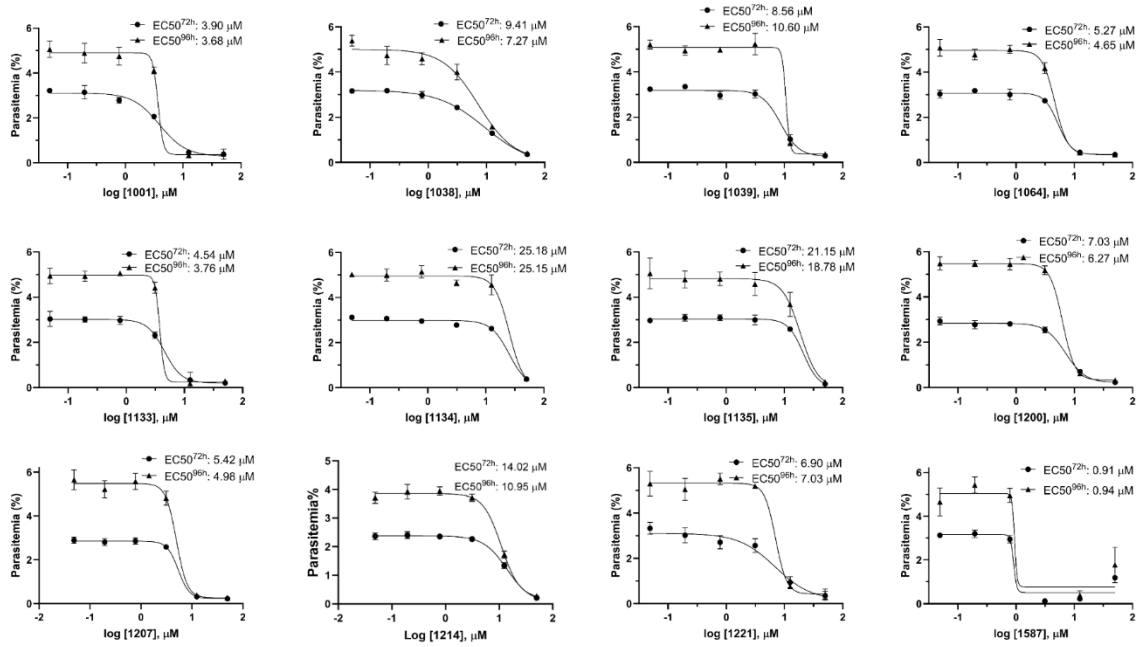

Figure 6. Testing phenylbenzoxazole (PBZ) GroEL inhibitors for anti-*Plasmodial* activity. *Wildtype* NF54 parasites were seeded at 0.5% parasitemia and incubated in serial dilutions of PBZ compounds, ranging from 50 µM to 50 nM. Parasitemia was measured after 72 or 96 hours to calculate the drugs' half-maximal effective concentrations (EC50). Data are fit to a dose-response equation and are represented as mean ± SEM.

Figure 7

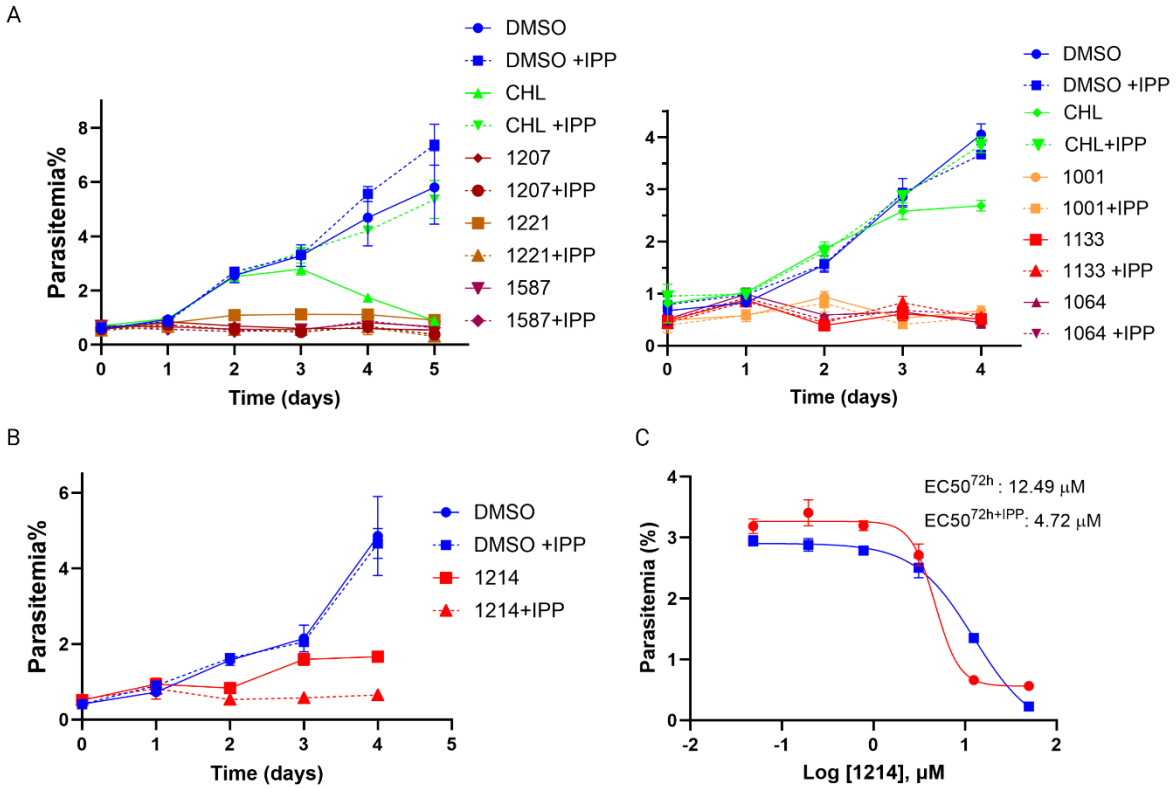

Figure 7. Testing specificity of PBZ compounds against apicoplast activity. A. *Wildtype* NF54 parasites were incubated with either DMSO (blue, control), 30µM Chloramphenicol (green, CHL) or 12.5µM of different PBZ compounds (shades of red), with (dashed) or without (solid) 200µM IPP. Parasitemia was monitored every 24 h over at least two cycles via flow cytometry. 100% of growth represents the highest value of calculated parasitemia (final parasitemia with DMSO). Normalized data are represented as mean ± SEM for three technical replicates. **B.** *Wildtype* NF54 parasites were incubated with DMSO (blue, control) or 12.5µM of PBZ1214 (red), with (dashed) or without (solid) 200µM IPP. Parasitemia was monitored every 24 h over two cycles via flow cytometry. Data are represented as mean ± SEM for three technical replicates. **C.** *Wildtype* NF54 parasites were seeded at 0.5% parasitemia and incubated in serial dilutions of PBZ1214 with (red) or without (blue) 200µM IPP. Parasitemia was measured after 72 hours to calculate the drugs' half-maximal effective concentrations (EC50). Data are fit to a dose-response equation and are represented as mean ± SEM.

Figure 8

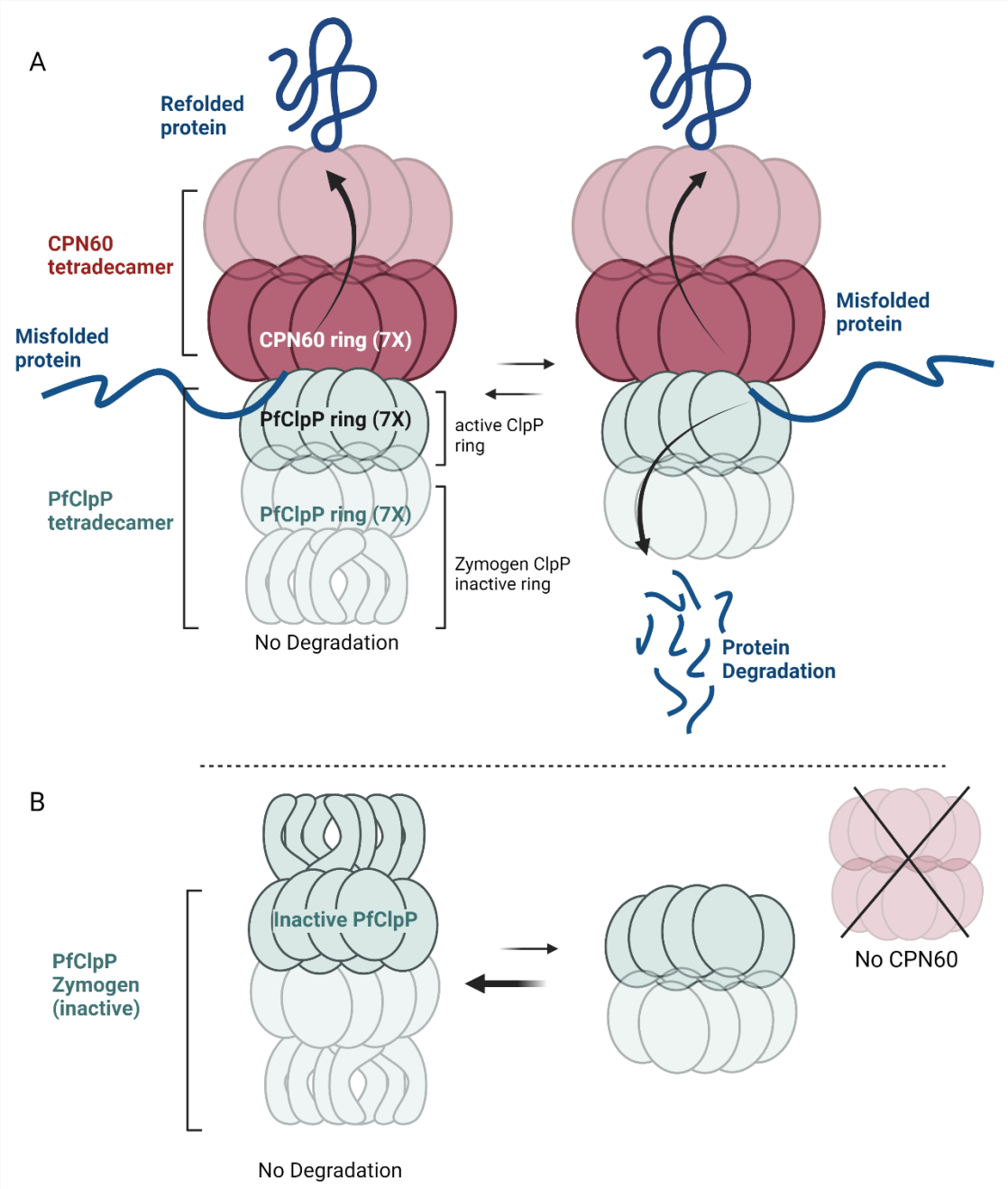

Figure 8: A model for regulation of proteostasis in the apicoplast by CPN and Clp complexes. A. Two opposing mechisms interact and balance proteostasis in the apicoplast; The CPN complex, consists of the ATPase chaperonin CPN60 which is arranged in two heptameric rings assisting in refolding organellar proteins. The Clp proteolytic complex in its core contains the PfClpP protease which is, likewise, arranged in two heptameric rings that degrade organellar proteins. PfClpP rings can be found in two forms; one as an inactive zymogen which contains an inhibitory pro-domain (left) and a processed form representing the proteolytically active ring (right). Both forms bind the CPN complex, however the binding to CPN60 is mediated by a PfClpP processed ring, predicting tetradecameric PfClpP complexes with a mix of inactive and active rings. The switch between the two forms enable a balance between

degradation and folding and determine the organellar proteostasis state. **B.** In the absence of CPN60, the PfClpP complex is balanced towards its inactive state and unable to initiate protein degradation. Thus, reduction in folding processes immediately triggers reduction in degradation to maintain proteostasis.

Sup Fig 1

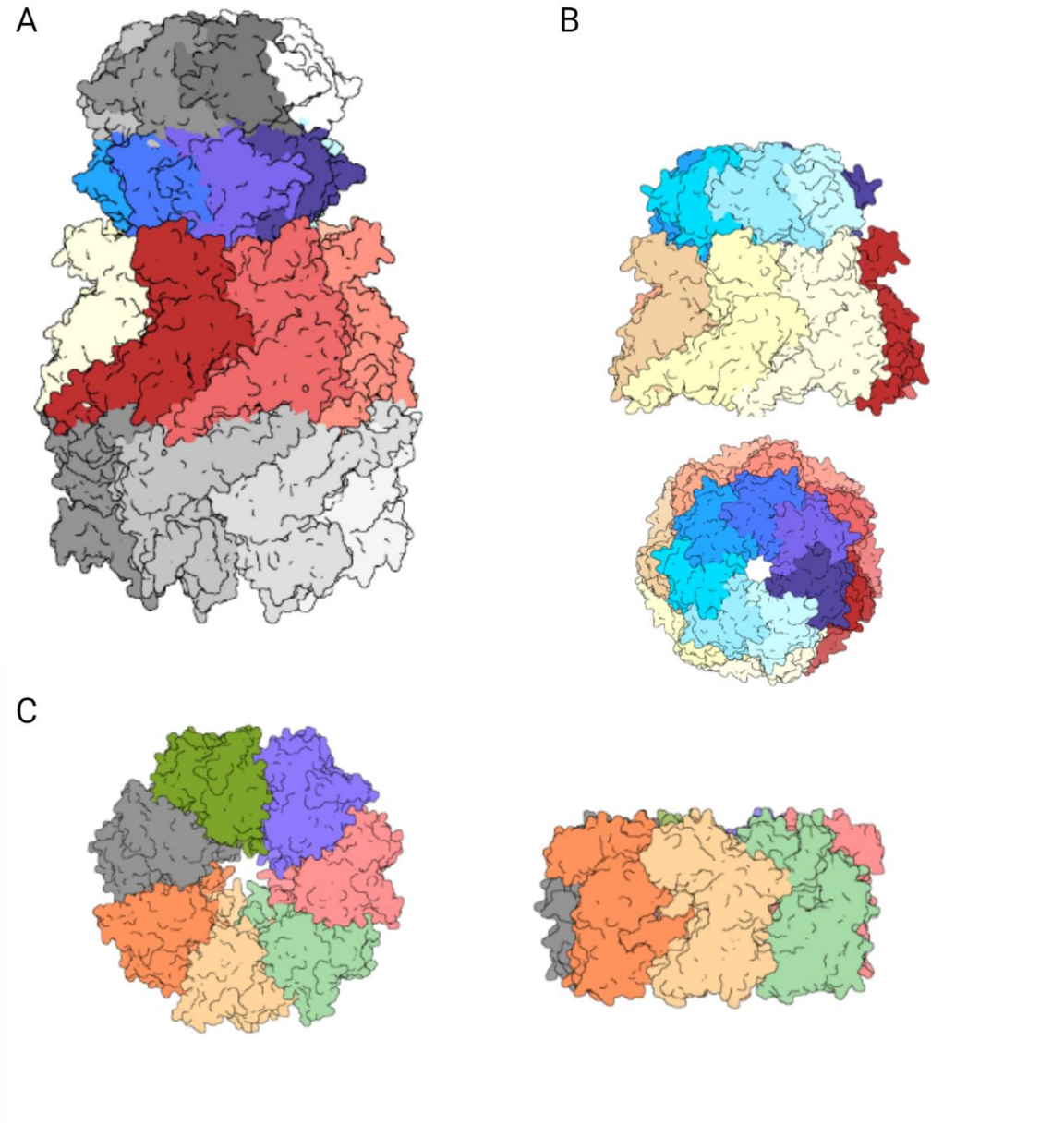

Sup. Fig. 1. A. A complete representation of the interaction between the two tetradecamers of CPN60 and PfClpP in the apicoplast. PfClpP is depicted in blue and teal shades, while CPN60 is colored in red, brown, and beige. A hypothetical model of the full tetradecamers, constructed based on the solved structures, is shown in grey tones (refer to Figure 5D). **B.** AF3 structure prediction of the interaction between the two heptameric rings of CPN60 and ClpP. The ClpP ring is shown tilting downward, binding to the upper side of CPN60. ClpP is depicted in blue and teal shades, while CPN60 is colored in red and beige. **C.** AF3 structure prediction of *Plasmodium falciparum* mitochondrial Hsp60. The different chains are highlighted in different colours, revealing the oligomeric arrangement of the complex.

Sup Fig 2

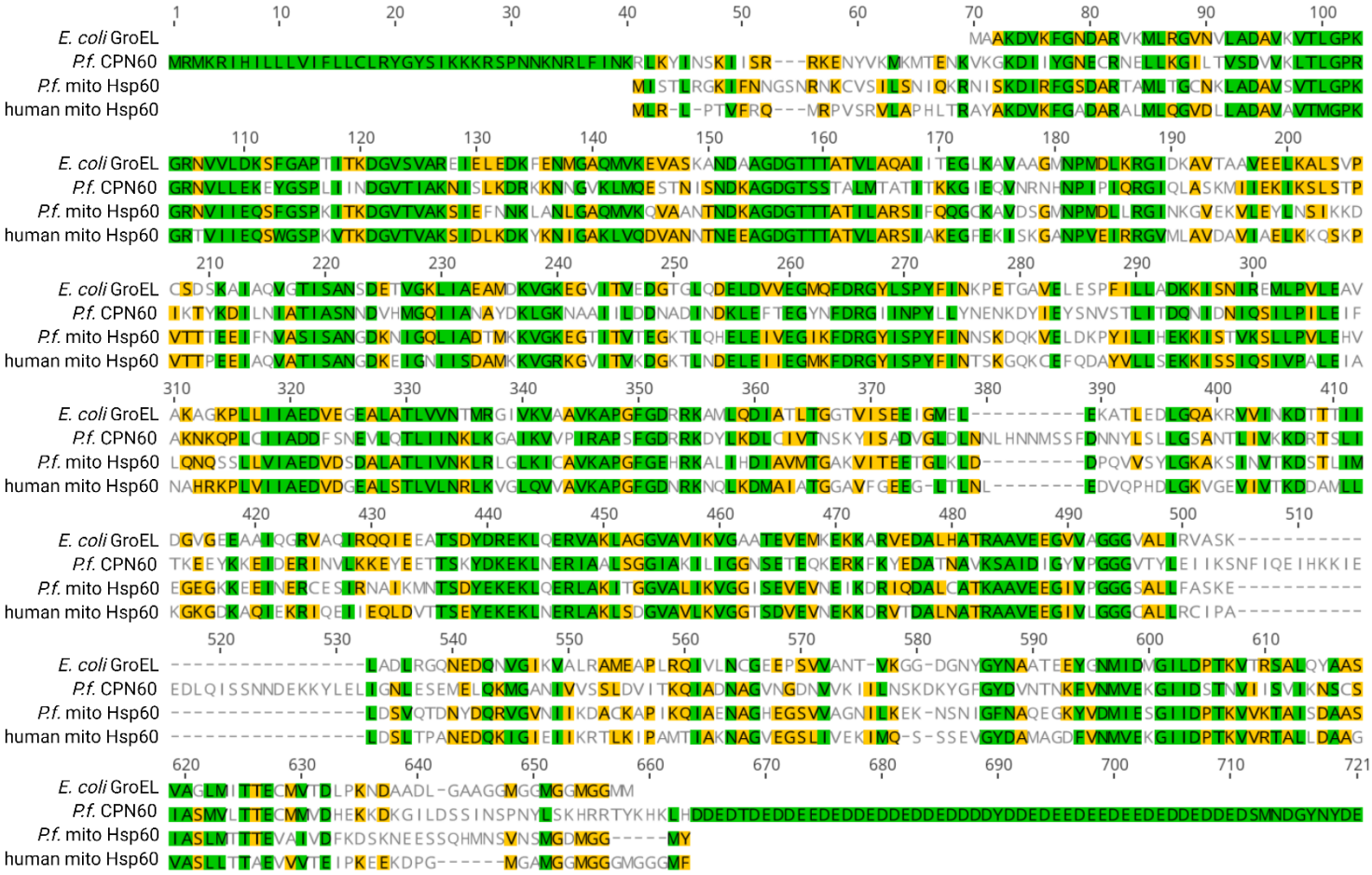

Sup. Fig. 2. Amino Acid sequence alignment between (1) *E. coli* GroEL (UNIPROT P0A6F5), (2) *Plasmodium falciparum* apicoplast CPN60 (PF3D7_1232100), (3) *Plasmodium falciparum* mitochondrial Hsp60 (PF3D7_1015600), and (4) human mitochondrial Hsp60 (UNIPROT P10809). Green represents Identity and high similarity (>80%) and Yellow similarity (>60%). Note the N-terminal extension of CPN60 representing the transit peptide which is removed upon apicoplast localization. Additional extensions appearing only in CPN60 are two inner loops and the long C-terminal stretch, which may interfere with PBZ binding.

Table 1

Table 1. PBZ compounds used in this study				
Test #	**Structure**	**#**	**EC_{50} Results (μM)**	
			72 h	**96 h**
1587	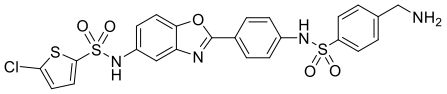	**PBZ 1587**	0.91	0.94
1038	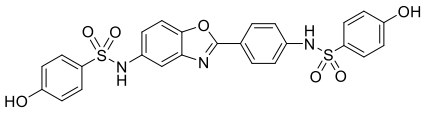	**PBZ 1038**	9.41	7.27
1001	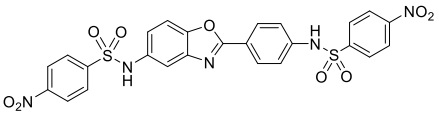	**1**	3.90	3.68
1064	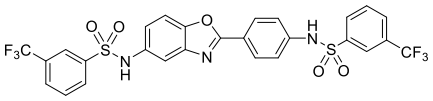	**2**	5.27	4.65
1133	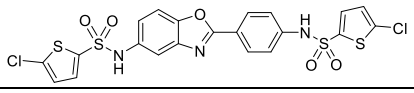	**3**	4.54	3.76
1135	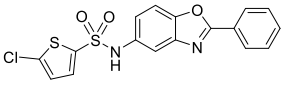	**3a**	21.15	18.78
1134	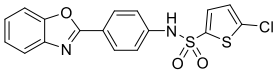	**3b**	25.18	25.15
1221	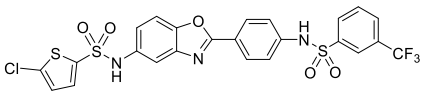	**4**	6.90	7.03
1039	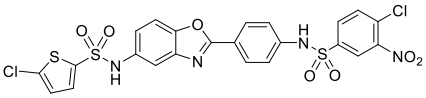	**5**	8.56	10.60
1200	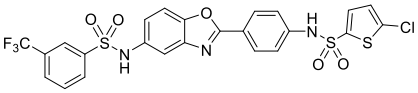	**6**	7.03	6.29
1207	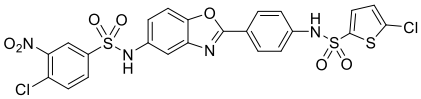	**7**	5.42	4.98
1214	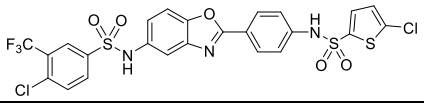	**8**	14.02	10.95

Table 2

Table 2: Primers and Oligos used in this study		
Primers	**Primer name**	**Primer sequence**
P1	Apt-CPN60-Cterm-EcoRV-F	TTTTTTTTGGATATCGAATCTGAAATGGAATTACAAAAAATGGGGGCTAATATAG
P2	CPN60 cterm apt R	TTGGTTTACCCTCGAGTTCATCATAATTGTATCCGTCGTTCATGCTATCTTCATCATC
P3	Apt-AflII-CPN60-3UTR-F	CTTTCCGGGCGCGCCTTAAGCACACATATATATATATATATATATATAAATTG
P4	CPN60-3UTR-EcoRV-Apt-R	TTCAGATTCGATATCCAAAAAAAACAAAAATTTTTATGTATTTATCCATATAC
P5	aptamer Forward	CTTATGACGTACCTGATTATGCAC
P6	aptamer Reverse	GTAGACCCCATTGTGAGTACATAAATATATTATATAAACTAGACTAGG
P7	CPN60 integr specific F	GTT CAA ATA ATG ACG AAA AGA AAT ATC TTG AAC TAA TAG G
P8	U6 CPN60 guide F	TAAGTATATAATATTGATGAAGATTCTATGAATGAGTTTTAGAGCTAGAA
P9	U6 CPN60 guide R	TTCTAGCTCTAAAACTCATTCATAGAATCTTCATCAATATTATATACTTA
P10	U6 HSP110 guide F	TAAGTATATAATATTGACAAACTTGGATGCAAATGGTTTTAGAGCTAGAA
P11	U6 HSP110 guide R	TTCTAGCTCTAAAACCATTTGCATCCAAGTTTGTCAATATTATATACTTA
P12	HSP110-Cterm pcr test F	GAGATCGTATTTTACTTTCCTTAGATGATTATGAAAATTGG
P13	HSP110-UTR pcr test R	GCATCAATGCACAAAATAAAAATCATACAATTTGGGG

References

1. Venkatesan, P. The 2023 WHO World malaria report. *Lancet Microbe* **5**, e214 (2024).

2. McFadden, G. I. *et al.* Plastid in human parasites. *Nature* **381**, 482–482 (1996).

3. Köhler, S. *et al.* A plastid of probable green algal origin in Apicomplexan parasites. *Science* **275**, 1485–1489 (1997).

4. Dooren, G. G. van & Striepen, B. The algal past and parasite present of the apicoplast. *Ann. Rev. Microbiol.* **67**, 271–289 (2013).

5. Ralph, S. A. *et al.* Metabolic maps and functions of the Plasmodium falciparum apicoplast. *Nat Rev Microbiol* **2**, 203–216 (2004).

6. Fichera, M. E. & Roos, D. S. A plastid organelle as a drug target in apicomplexan parasites. *Nature* **390**, 407–409 (1997).

7. Biddau, M. & Sheiner, L. Targeting the apicoplast in malaria. *Biochem. Soc. Trans.* **47**, 973–983 (2019).

8. Waller, R. F., Reed, M. B., Cowman, A. F. & McFadden, G. I. Protein trafficking to the plastid of Plasmodium falciparum is via the secretory pathway. *Embo J* **19**, 1794–1802 (2000).

9. Foth, B. J. *et al.* Dissecting Apicoplast Targeting in the Malaria Parasite Plasmodium falciparum. *Science* **299**, 705–708 (2003).

10. Swift, R. P. *et al.* A mevalonate bypass system facilitates elucidation of plastid biology in malaria parasites. *PLoS Pathog.* **16**, e1008316 (2020).

11. Yeh, E. & DeRisi, J. L. Chemical Rescue of Malaria Parasites Lacking an Apicoplast Defines Organelle Function in Blood-Stage Plasmodium falciparum. *PLoS Biol.* **9**, e1001138 (2011).

12. Walczak, M., Ganesan, S. M., Niles, J. C. & Yeh, E. ATG8 Is Essential Specifically for an Autophagy-Independent Function in Apicoplast Biogenesis in Blood-Stage Malaria Parasites. *Mbio* **9**, e02021-17 (2018).

13. Swift, R. P., Rajaram, K., Liu, H. B. & Prigge, S. T. Dephospho-CoA kinase, a nuclear-encoded apicoplast protein, remains active and essential after Plasmodium falciparum apicoplast disruption. *Embo J.* e107247 (2021) doi:10.15252/embj.2020107247.

14. Florentin, A. *et al.* PfClpC Is an Essential Clp Chaperone Required for Plastid Integrity and Clp Protease Stability in Plasmodium falciparum. *Cell Rep.* **21**, 1746–1756 (2017).

15. Florentin, A., Stephens, D. R., Brooks, C. F., Baptista, R. P. & Muralidharan, V. Plastid biogenesis in malaria parasites requires the interactions and catalytic activity of the Clp proteolytic system. *Proc. Natl. Acad. Sci.* **3**, 201919501 (2020).

16. Schirmer, E. C., Glover, J. R., Singer, M. A. & Lindquist, S. HSP100/Clp proteins: a common mechanism explains diverse functions. *Trends. biochem. Sci.* **21**, 289–296 (1996).

17. Nishimura, K. & Wijk, K. J. van. Organization, function and substrates of the essential Clp protease system in plastids. *Biochimica et Biophysica Acta (BBA) - Bioenergetics* **1847**, 915–930 (2015).

18. Bouchnak, I. & Wijk, K. J. van. Structure, Function and Substrates of Clp AAA+ protease systems in cyanobacteria, plastids and apicoplasts; a comparative analysis. *J Biol Chem* **296**, 100338 (2021).

19. Olinares, P. D. B., Kim, J., Davis, J. I. & Wijk, K. J. van. Subunit Stoichiometry, Evolution, and Functional Implications of an Asymmetric Plant Plastid ClpP/R Protease Complex in Arabidopsis. *Plant Cell* **23**, 2348–2361 (2011).

20. Kim, J. *et al.* Subunits of the Plastid ClpPR Protease Complex Have Differential Contributions to Embryogenesis, Plastid Biogenesis, and Plant Development in Arabidopsis. *The Plant Cell* **21**, 1669–1692 (2009).

21. Bakkouri, M. E. *et al.* Structural insights into the inactive subunit of the apicoplast-localized caseinolytic protease complex of Plasmodium falciparum. *J. Biol. Chem.* **288**, 1022–1031 (2013).

22. Bakkouri, M. E. *et al.* The Clp Chaperones and Proteases of the Human Malaria Parasite Plasmodium falciparum. *J. Mol. Biol.* **404**, 456–477 (2010).

23. Singh, M. K. *et al.* Molecular Chaperonin HSP60: Current Understanding and Future Prospects. *Int. J. Mol. Sci.* **25**, 5483 (2024).

24. Dupuy, E. & Collet, J.-F. Entering deeper into the mysteries of the GroEL–GroES nanomachine. *Curr. Opin. Microbiol.* **79**, 102480 (2024).

25. Perez, R. F., Mochi, G., Khan, A. & Woodford, M. Mitochondrial Chaperone Code: Just warming up. *Cell Stress Chaperones* **29**, 483–496 (2024).

26. Fellows, J. D., Cipriano, M. J., Agrawal, S. & Striepen, B. A Plastid Protein That Evolved from Ubiquitin and Is Required for Apicoplast Protein Import in Toxoplasma gondii. *mBio* **8**, 10.1128/mbio.00950-17 (2017).

27. Ganesan, S. M., Falla, A., Goldfless, S. J., Nasamu, A. S. & Niles, J. C. Synthetic RNA-protein modules integrated with native translation mechanisms to control gene expression in malaria parasites. *Nat. Commun.* **7**, 10727 (2016).

28. Elaagip, A., Absalon, S. & Florentin, A. Apicoplast Dynamics During Plasmodium Cell Cycle. *Front. Cell. Infect. Microbiol.* **12**, 864819 (2022).

29. Dahl, P. J. & Rosenthal, E. L. Multiple Antibiotics Exert Delayed Effects against the Plasmodium falciparum Apicoplast. *Antimicrob. Agents Chemother.* **51**, 3485–3490 (2007).

30. Nguyen, B., Ma, R., Tang, W. K., Shi, D. & Tolia, N. H. Crystal structure of P. falciparum Cpn60 bound to ATP reveals an open dynamic conformation before substrate binding. *Sci. Rep.* **11**, 5930 (2021).

31. Abramson, J. *et al.* Accurate structure prediction of biomolecular interactions with AlphaFold 3. *Nature* **630**, 493–500 (2024).

32. Jumper, J. *et al.* Highly accurate protein structure prediction with AlphaFold. *Nature* **596**, 583–589 (2021).

33. Johnson, S. M. *et al.* A biochemical screen for GroEL/GroES inhibitors. *Bioorg. Med. Chem. Lett.* **24**, 786–789 (2014).

34. Godek, J. *et al.* Bis-sulfonamido-2-phenylbenzoxazoles Validate the GroES/EL Chaperone System as a Viable Antibiotic Target. *J. Am. Chem. Soc.* **146**, 20845–20856 (2024).

35. Gruber, A. V. & Feiz, L. Rubisco Assembly in the Chloroplast. *Front. Mol. Biosci.* **5**, 24 (2018).

36. Sheiner, L. *et al.* A Systematic Screen to Discover and Analyze Apicoplast Proteins Identifies a Conserved and Essential Protein Import Factor. *PLoS Pathog.* **7**, e1002392 (2011).

37. Elaagip, A., Absalon, S. & Florentin, A. Apicoplast dynamics during Plasmodium cell cycle. *Front. Cell. Infect. Microbiol. Parasite and Host* (2022).

38. Chappell, L. *et al.* Refining the transcriptome of the human malaria parasite Plasmodium falciparum using amplification-free RNA-seq. *BMC Genom.* **21**, 395 (2020).

39. Bowman, J. D. *et al.* Antiapicoplast and Gametocytocidal Screening To Identify the Mechanisms of Action of Compounds within the Malaria Box. *Antimicrob. Agents Chemother.* **58**, 811–819 (2014).

40. Boucher, M. J. & Yeh, E. Disruption of Apicoplast Biogenesis by Chemical Stabilization of an Imported Protein Evades the Delayed-Death Phenotype in Malaria Parasites. *mSphere* **4**, 10.1128/msphere.00710-18 (2019).

41. Amberg-Johnson, K. *et al.* Small molecule inhibition of apicomplexan FtsH1 disrupts plastid biogenesis in human pathogens. *eLife* **6**, e29865 (2017).

42. Pires, C. V., Chawla, J., Simmons, C., Gibbons, J. & Adams, J. H. Heat-shock responses: systemic and essential ways of malaria parasite survival. *Curr. Opin. Microbiol.* **73**, 102322 (2023).

43. Tintó-Font, E. & Cortés, A. Malaria parasites do respond to heat. *Trends Parasitol.* **38**, 435–449 (2022).

44. Harbut, M. B. *et al.* Targeting the ERAD pathway via inhibition of signal peptide peptidase for antiparasitic therapeutic design. *Proc. Natl. Acad. Sci.* **109**, 21486–21491 (2012).

45. Zhang, M. *et al.* The apicoplast link to fever-survival and artemisinin-resistance in the malaria parasite. *Nat. Commun.* **12**, 4563 (2021).

46. Gersch, M. *et al.* AAA+ chaperones and acyldepsipeptides activate the ClpP protease via conformational control. *Nat. Commun.* **6**, 6320 (2015).

47. Abdeen, S. *et al.* GroEL/ES inhibitors as potential antibiotics. *Bioorg. Med. Chem. Lett.* **26**, 3127–3134 (2016).

48. Zimbone, S., Rosa, M. C. D., Chiechio, S. & Giuffrida, M. L. Exploring the Role of Hsp60 in Alzheimer's Disease and Type 2 Diabetes: Suggestion for Common Drug Targeting. *Int. J. Mol. Sci.* **24**, 12456 (2023).

49. Bavisotto, C. C. *et al.* Hsp60 Post-translational Modifications: Functional and Pathological Consequences. *Front. Mol. Biosci.* **7**, 95 (2020).

50. Washburn, A. *et al.* Dual-targeting GroEL/ES chaperonin and protein tyrosine phosphatase B (PtpB) inhibitors: A polypharmacology strategy for treating Mycobacterium tuberculosis infections. *Bioorg. Med. Chem. Lett.* **29**, 1665–1672 (2019).

51. Abdeen, S. *et al.* Targeting the HSP60/10 chaperonin systems of Trypanosoma brucei as a strategy for treating African sleeping sickness. *Bioorg. Med. Chem. Lett.* **26**, 5247–5253 (2016).

52. Leitner, A. *et al.* The Molecular Architecture of the Eukaryotic Chaperonin TRiC/CCT. *Structure* **20**, 814–825 (2012).

53. Lu, K.-Y. *et al.* Plasmodium chaperonin TRiC/CCT identified as a target of the antihistamine clemastine using parallel chemoproteomic strategy. *Proc. Natl. Acad. Sci.* **117**, 5810–5817 (2020).

54. Spillman, N. J., Beck, J. R., Ganesan, S. M., Niles, J. C. & Goldberg, D. E. The chaperonin TRiC forms an oligomeric complex in the malaria parasite cytosol. *Cell. Microbiol.* **19**, e12719 (2017).

55. Mbengue, A. *et al.* New Export Pathway in Plasmodium falciparum-Infected Erythrocytes: Role of the Parasite Group II Chaperonin, PfTRiC. *Traffic* **16**, 461–475 (2015).

56. Muralidharan, V., Oksman, A., Iwamoto, M., Wandless, T. J. & Goldberg, D. E. Asparagine repeat function in a Plasmodium falciparum protein assessed via a regulatable fluorescent affinity tag. *Proc. Natl. Acad. Sci.* **108**, 4411–4416 (2011).

57. Kudyba, H. M., Cobb, D. W., Florentin, A., Krakowiak, M. & Muralidharan, V. CRISPR/Cas9 Gene Editing to Make Conditional Mutants of Human Malaria Parasite P. falciparum. *J. vis. Exp. JoVE* (2018) doi:10.3791/57747.

58. Muralidharan, V., Oksman, A., Pal, P., Lindquist, S. & Goldberg, D. E. Plasmodium falciparum heat shock protein 110 stabilizes the asparagine repeat-rich parasite proteome during malarial fevers. *Nat. Commun.* **3**, 1310 (2012).

59. Kortemme, T., Kim, D.E., and Baker, D. Computational alanine scanning of protein-protein interfaces. Sci. STKE. pl2. (2004).